WIND TUNNEL INVESTIGATIONS OF MODEL ROTOR NOISE AT LOW TIP SPEEDS*

K. S. Aravamudan, A. Lee, and W. L. Harris
Massachusetts Institute of Technology

SUMMARY

This paper summarizes the experimental and related analytical results on model rotor rotational and broadband noise obtained at M.I.T. since 1975. The objectives of this research program have been to define the various noise sources, to determine the effects of helicopter performance parameters on the noise generated by a model main rotor, and to derive appropriate scaling laws for the various types of main rotor noise.

A description of the M.I.T. anechoic wind tunnel and rotor facility and some of the findings of this research group have been reported previously. The parameters under study were the variation of helicopter performance parameters such as number of blades, blade pitch (thrust), and advance ratio. In addition, the research program has consisted of an examination of the effects of intensity and size scales of injested turbulence on the intensity and spectra of broadband noise.

INTRODUCTION

Helicopter rotors generate complex acoustic signatures. A variety of mechanisms are responsible for the radiated acoustic energy and only a few of these mechanisms are understood.

The sound radiated by a lifting rotor at low to moderate tip speeds is essentially due to the time varying pressure distributions on the blade. This, often termed as "rotational noise", was originally studied by Gutin [1]†, where only steady, azimuthally constant blade loads were considered. These discrete frequency components occur at multiples of blade passage frequency and the unsteady nature of the blade forces prevents the harmonics from decaying, as originally predicted by Gutin. Random noise formerly was called "vortex noise," but investigators now prefer "broadband noise" since vortex shedding itself is not believed to be the principal mechanism.

At higher tip speeds and/or high flight speed, the flow over the blade section may exceed sonic velocity and result in generation of a local shock. These are termed as "shock noise" and are characterized by sharp peaks in the acoustic pressure time history, resulting in highly annoying banging noise.

*This research program has been supported by the U.S. Army, Army Research Office, under contract DAAG29-76-C-0027.

†Numbers in brackets indicate reference numbers.

Another dominant noise source is due to "blade-vortex interaction." A blade that passes close to a wake vortex filament experiences [2,3] a rapid change in the aerodynamic loading. This, often termed as "blade slap," is dependent on the geometry of the wake. Both these noise sources are impulsive in nature and occur only at certain flight conditions of a helicopter. In the absence of these mechanisms, the discrete and broadband noise dominate the rotor noise spectra.

Whereas the rotational or discrete noise from the rotors is fairly well understood, the situation for broadband noise is most unsatisfactory. Almost nothing can be said unequivocally about the broadband noise and this is simply because of the difficulty in pinpointing the noise sources experimentally. Opinions regarding the origins and behavior of broadband noise vary somewhat among investigators, but there is general agreement that turbulence in the flow seen by rotor blades is the basic physical mechanism responsible for broadband noise. Recent experimental data for a full scale helicopter rotor obtained by Leverton [4] and Leverton and Pollard [5] seem to suggest that the broadband noise is dependent only on the nature of turbulence. Thus, the turbulence may be due to inflow, the boundary layer of the blades, or the wake itself and may generate an unsteady lift on the airfoil and hence the noise. Principal areas of uncertainty include the effects of velocity and the size scale of turbulence on the intensity and spectra of the broadband noise. The work of Leverton [4] fails to show any kind of Strouhal frequency scaling with velocity for full scale rotors.

Much of the recent impetus to study the rotational and broadband noise comes from improved data processing technique and equipment. Narrowband analysis of rotor noise data has shown discrete frequency components extending well beyond 150 Hz, which historically was believed to be the transition region between rotational noise and broadband noise for typical helicopter rotors. Work by Lowson, Whatmore, and Whitfield [6] and by Leverton [4] emphasizes that low frequency broadband noise could have different causative physical mechanisms and acoustic behavior than high frequency broadband noise. It is generally believed that the inflow turbulence interaction with the rotor blades is responsible for the low frequency broadband noise. The high frequency component is attributed to the vortex shedding by the airfoils. In Figure 1 is shown a typical 6% bandwidth acoustic spectrum of a model rotor. Identified in this figure are the regions of rotational noise, low frequency broadband noise, and high frequency broadband noise.

To obtain the relationship between flow field characteristics and the sound radiated by lifting rotors, it is necessary to determine which mechanism is primarily responsible for the radiation. Each postulated mechanism leads to a particular characterization of the sound field and of its relationship to the flow field characteristics. Empirical measurements and similarity arguments can then be used to establish a posteriori verification of the choice of the mechanism. To this end, we assume that (i) the steady and unsteady loading harmonics are responsible for radiation of rotational noise, (ii) the intensity and size scale of turbulence are the governing factors for low frequency broadband noise radiation, and (iii) the periodic vortex shedding is

the dominant mechanism responsible for radiation of high frequency broadband noise. The major contribution of the research effort described in this report is the development of appropriate Mach number scaling laws for model helicopter rotor noise and experimental verification of these laws. Equally important has been the obtainment of a definition of the effects of helicopter performance parameters on model helicopter rotor noise. These latter effects have been reported previously by references 7, 8, and 9.

Here, an attempt has been made to study the influence of free stream disturbances on the acoustic signatures generated by a model helicopter rotor. Appropriate theoretical modelling for rotational noise, low frequency broadband noise, and high frequency broadband noise are made by exploiting the existing knowledge of acoustic radiation from a rotating dipole source and unsteady aerodynamics associated with rotating blades. Details of the experimental facility and the theoretical analysis may be found in a recent report by Aravamudan and Harris [7] and several other archival publications of the members of the Fluid Dynamics Research Laboratory of M.I.T. [8 and 9].

In the section entitled "Description of Experiments," a brief description of the M.I.T. anechoic wind tunnel and model rotor facility is presented, along with the instrumentation used for acquisition and processing of various rotor noise components. Here we have discussed the nature of the artificially generated tunnel turbulence and the appropriate theoretical modelling of its spectrum.

In the section entitled "Mach Number Scaling of Model Rotor Noise," a simple Mach number scaling procedure is derived to predict the intensity and spectra of various components of model rotor noise, and the computed and the measured results are compared and described. The conclusions of our efforts are discussed in the Conclusion section.

DESCRIPTION OF EXPERIMENTS

The M.I.T. anechoic wind tunnel facility was used to study the rotational and broadband noise components of a model rotor. Controlled turbulence of varying intensity and scale was generated at the inlet of the tunnel test section by inserting biplanar grids of different sizes in the tunnel contraction section. In this section, the experimental apparatus used in obtaining and analyzing both turbulence and acoustic data is described.

The M.I.T. Anechoic Tunnel and Rotor Facility

The wind tunnel has a 1.52 x 2.29 meter inlet open jet test section which is enclosed in a 3.65 x 3.65 x 7.3 meter anechoic chamber. The sides of the chamber were covered with Cremer Blocks and the floor of the chamber was covered with 15-cm thick polyurethene foam. The anechoic properties of the tunnel were measured and the acoustic cut-off frequency above which free field conditions prevail was found to be 160 Hz. The effects of the shear layer of the open jet on refraction and scattering of acoustic waves were studied by using aeolian tones as a sound source and were found to be insignificant under the present test conditions.

The model helicopter rotor system consists of a 1.27 meter diameter rotor and has blades made of fiberglass. The rotor hub is designed to take up to 8 blades and is connected to a thrust measuring dynamometer. The dynamometer consists of four sets of BLH SPB 3-20-35 semiconductor strain gages mounted on two sets of flexures. Lebow slip ring was used to transmit the signals from the rotating dynamometer. The details of the model rotor system are summarized in Table 1.

Instrumentation

Data flow for all the experiments performed for this study was from microphones and hot wire sensors to a magnetic tape and later from the magnetic tape to appropriate spectrum analyzers.

The acoustic measurements were made along a circular arc at a radius of 1.32 meters from the rotor disc plane, perpendicular to the direction of the wind, and passing through the axis of the rotor. Acoustic signals were measured using a 1/2 inch B & K microphone type 4133 with a cathode follower type 2614 (1/2 in. = 1.27 cm). The signals were amplified by a B & K microphone amplifier and were recorded on magnetic tape using a P.I. 4 channel tape recorder model 6204 in direct mode. The microphones were calibrated using a B & K piston phone type 4220. In addition to the acoustic signal, a timing pulse at a period of 1/B Ω was also recorded on one of the channels of the tape recorder. The steady thrust measurements were made simultaneously with the aid of a digital volt meter.

The fluctuating velocity signals were measured with an X-type hot wire sensor type DISA 55P51. The probe was placed 19 cm directly above the rotor plane, 10 cm aft the axis of the rotor. Flow Corporation constant temperature anemometer type 900-1 was used in conjunction with Flow Corporation linearizers type 900-4 and type 4835-C. An attenuator was used with the latter linearizer in order to adjust the sensitivity of both the wires to be same. The probe was calibrated over anticipated test velocities and the responses of both wires were found linear. The linearized signals were processed through a Flow Corporation sum and difference unit to yield the longitudinal and vertical components of velocities. These signals were further passed through a Flow Corporation suppressor filter unit type 900-3 to yield only the fluctuating quantities of the signal. All the signals were constantly monitored with the aid of a Flow Corporation digital volt meter type 900-2D. The fluctuating signals were then recorded on two F.M. channels of a P.I. 4 channel tape recorder type 6204. The r.m.s. values of the signals were measured by using HP 3400A RMS volt meters. In Figure 2 a schematic of instrumentation used in acquisition of turbulence and acoustic data is shown. The acoustic, thrust, and turbulence measurements were made simultaneously.

The measured acoustic signals were processed with the aid of a B & K audio frequency analyzer type 2107 and a B & K graphic level recorder. The turbulence data were analysed with the aid of a Federal Scientific UA-15A Spectrum analyzer together with a 1015 averager.

Turbulence and Acoustic Measurements

The grids employed in this study were designed based on the data of Baines and Peterson [10]. The grids were biplanar consisting of bars of 1.91 cm with a mesh size of 15 cm and bars of 8.9 cm with a mesh size of 50.8 cm. The grid solidities were 0.23 and 0.32, respectively. The grid Reynolds numbers based on the lowest tunnel velocity were 9×10^4 and 3×10^5, respectively. The longitudinal and vertical integral scales Λ_f and Λ_g of the grid generated turbulence were determined near the axis of rotor. For convenience, we estimated Λ_f from the Eulerian integral time scale τ_e. The values of τ_e were determined from the extrapolated zero intercept of the power spectra of longitudinal and vertical velocities. The length scales, then, are given by

$$\Lambda_f = U_0 \tau_{ef} \; ; \quad \Lambda_g = U_0 \tau_{eg} \tag{1}$$

The measured longitudinal and vertical integral scales of grid generated turbulence were observed to be independent of free stream velocity. In absence of grids, the Eulerian time scales were very large and fluctuating. This resulted in large length scales that vary considerably with free stream velocity, but do not follow any definite pattern. Details of these measurements are presented by Aravamudan and Harris [7]. Table 2 summarized the measured characteristics of turbulence with and without the grids.

In Figures 3 and 4 are the measured power spectral densities of the longitudinal and vertical components of turbulence, respectively, as a function of wave number. In plotting these figures, Taylor's hypothesis of frozen turbulence has been applied to convert the turbulence spectrum from an experimentally obtained temporal frame to a spatial frame. The axial wave number is related to frequency by $k_x = 2\pi f/U_0$ and this is nondimensionalized with respect to k_e as $3k_x/8\pi k_e$. Here k_e is the wave number range of energy containing eddies and is related to the longitudinal integral scale Λ_f by $k_e \simeq 0.75/\Lambda_f$. Also shown in the figures is the empirical isotropic turbulence spectrum derived from von Karman's interpolation formula. The nondimensionalized power spectral densities for longitudinal and vertical components of turbulence are given as follows

$$\Phi_{uu}(k_x) = \Phi_{uu}(o)/[1 + k_x^2/k_e^2]^{5/6} \tag{2}$$

$$\Phi_{ww}(k_x) = \frac{\Phi_{ww}(o)[1 + 8/3\, k_x^2/k_e^2]}{[1 + k_x^2/k_e^2]^{11/6}} \tag{3}$$

The measured data show good agreement with the von Karman spectrum, including a -5/3 power decrease at high frequencies. However, in the absence of grids, the tunnel turbulence seems to deviate slightly from the predicted von Karman power spectrum.

Extensive measurements of the background noise for the M.I.T. anechoic wind tunnel facility have been made by Harris and Lee [11]. However, it is very likely that an upstream turbulence generator would alter the background noise spectra of the tunnel. To ensure that the acoustic measurements were not affected by such noise, a survey of the tunnel background noise was made at various tunnel speeds with and without the turbulence generating grids in place.

To isolate the low frequency rotational noise components of the rotor from the relatively high intensity tunnel background noise, a periodic sampling technique was used. This technique involves the use of a PAR wave-form eductor, Model TDH-9. The waveform eductor samples the repetitive input and stores them in a 100 channel capacitance memory. After a sufficient number of sweeps have occurred, the noise from nonrepetitive sources (background noise in the present case) will be suppressed since their average value will approach zero. The processed rotor data will contain only the rotational noise. The timing pulse of 1/BΩ was used to average the waveform of the signal. The spectrum was obtained by using a Federal Scientific UA-15A Spectrum Analyzer with a 1015 averager.

Since the present study also involves the influence of free stream disturbances on the low frequency broadband noise sources, it was necessary to ensure that (i) the rotational harmonics do not contribute significantly to the broadband noise generated by the rotor and (ii) the background noise level in the tunnel is low enough to yield the necessary signal to noise ratio. The first task was accomplished with the use of the above mentioned periodic sampling technique.

In Figure 5 are plotted the 6% bandwidth spectra for a two-bladed rotor operating at 672 rpm and an advance ratio of 0.3. The 1.91 cm x 15 cm turbulence generating grid was located upstream and the Figure compares the spectra obtained with and without periodic sampling technique. The rotational harmonics obtained from the periodic sampling technique are very distinct and they decay very rapidly. As can be seen from Figure 5, above 200 Hz, which we assume as the transition from rotational noise to broadband noise, the levels of broadband noise are significantly higher than those of rotational harmonics.

The second task was accomplished by measuring the acoustic signals at a given observer location with and without the rotor system operating. Figures 6 and 7 show the measured 6% bandwidth sound pressure levels for 1.91 cm x 15 cm grid and 8.9 cm x 50.8 cm grid, respectively. Also drawn in these figures are the typical noise spectra with the model rotor operating in the tunnel. From Figures 6 and 7, it is evident that the background noise in the wind tunnel does not affect the rotor generated broadband noise. In the absence of turbulence generating grids, the background noise of the wind tunnel seems comparable to the intensity of low frequency broadband noise. Hence, we have not used this experimentally obtained low frequency broadband noise data in our prediction techniques.

MACH NUMBER SCALING OF MODEL ROTOR NOISE

As mentioned above, the acoustic spectra generated by a typical rotor may be decomposed into rotational noise, low frequency broadband noise, and high frequency broadband noise components. The intensity and spectral content of each of these components are strongly dependent on the blade tip Mach number. Most model rotor systems can not simulate the high tip Mach numbers of real helicopters and hence there is a need for a simple prediction procedure based on the blade tip Mach number and other performance parameters. In this section, we have attempted to use the existing theories of radiation from subsonic rotors to yield a simplified Mach number scaling formula for the intensity and spectra of various components of model rotor noise. Due to nature of this article, we have deliberately abstained from presenting the complex mathematical development of the scaling procedures but confine ourselves to discussions of relevant assumptions and the final scaling formulae. Similarly, our findings on the effects of helicopter performance parameters on model helicopter rotor noise will not be presented in this paper.

Mach Number Scaling of Rotational Noise Component

The rotational noise of subsonic rotors is mainly attributed to force and thickness effects. The relative importance of force and thickness effects depends strongly on the blade Mach number. The source strength of the force term is larger than that of the thickness term. However, the acoustic efficiency of the thickness source radiation is far greater than that due to the force. Thus, which mechanism dominates the acoustic field is essentially a question of whether the added acoustic efficiency of the thickness source can overcome its inherently weak strength. Since the acoustic efficiency decays rapidly with decreasing Mach number, there is a rapid fall-off in acoustic effectiveness for blade stations inboard of the tip. Hence, in the following order-of-magnitude considerations on the force and thickness effects, only tip regions need to be considered.

For each source, its effective Mach number $M_e = M_t \sin\alpha/(1-M_{or})$ is maximum in a direction straight ahead of the rotor. The factor $(1-M_{or})$ is minimum for the advancing blade and hence the sources in the vicinity of the advancing blade contribute more. The front rotor disc plane is chosen as the observer location since the thickness noise is most intense in this location. We further assume that the tip Mach numbers are below the critical Mach numbers and hence compressibility corrections are omitted. Hawkings and Lowson [12] found the acoustic source strength of thickness, direct force, and force derivative terms to be of the order of $\rho_0\Omega^2$ t, $\Omega F_r/c_0$, and $1/c_0(\partial F_r/\partial\tau)$. The thickness source term $\rho_0\Omega^2 t$ may be rewritten as $(\rho_0 c_0\Omega)$ $(M_t\ c/b)(t/c)$. Ignoring the directional properties of F_r, one can rewrite the second term as $1/2\ C_f M_s^2(\rho_0 c_0\Omega)$ where $M_s = (1+\mu)M_t$ for the advancing blade. Based on quasi-steady approximations, Hawkings and Lowson [12] suggested an order of $0.1\ \rho_0 c_0\Omega$ for force derivative term. For typical helicopter rotors, $b/c \approx 12$, $t/c \approx 0.12$, $C_f \approx 0.06$, and the order of magnitude of these sources is $0.01\ M_t\rho_0 c_0\Omega$, $0.03\ M_s^2\rho_0 c_0\Omega$, and $0.1\rho_0 c_0\Omega$, respectively. Based on calculations of Hawkings and Lowson, the approximate expressions for the acoustic efficiency

of each of these sources are given by $2.6 \times 10^4 M_e^{11.4}/(1- M_1)^3$, $2.2 \times 10^2 M_e^{8.4}/(1 - M_1)^2$ and $1.8 \times 10^2 M_e^{6.3}/(1-M_1)^2$, respectively. Combining the source strength and its acoustic efficiency, the ratio of acoustic pressure due to thickness, force, and force derivative is given as follows:

$$260\ M_e^{6.1} : 6.6\ M_s^2\ M_e^{2.1} : 18$$

For a typical helicopter with an advance ratio of 0.3, $M_e = 0.6$, $M_s = 0.65$, and the second term is of the order of unity. The thickness and force derivative terms are equally important at a value of $M_e = 0.65$ where both the terms are of same order. However, as the Mach number is decreased to about 0.60, the thickness term is about 4 dB less than the corresponding force derivative term and at $M_e = 0.5$, it is about 14 dB less. Hence, in our Mach number scaling formulation, we need consider only force derivative terms and the formulation would still be valid for relatively high up Mach numbers; the tip Mach number is limited by 0.65.

Lowson and Ollerhead [13] derived the expressions for the farfield acoustic radiation due to a rotating fluctuating point source in terms of an infinite sum of loading harmonics due to thrust, drag, and centrifugal forces. For a typical helicopter rotor, the proportions of thrust, drag, and radial forces are of the order of 10:1:1. Further, the complex Fourier coefficient consisting of two Bessels functions of order $(n + \lambda)$ and $(n - \lambda)$ may readily be interpreted as representing rotational modes of $n\Omega/(n + \lambda)$ and $n\Omega/(n - \lambda)$, respectively. Since faster modes have higher efficiency, the contributions of slower modes may be ignored. Under such assumptions, the complex Fourier coefficient for sound radiation from a source at a distance R from axis of rotation will be simplified to the following expression:

$$C_n = \sum_{\lambda=0}^{\infty} \frac{(i)^{-(n-\lambda)}}{4\pi} \frac{n\Omega x}{c_0 r_1^2} [i\, a_{\lambda T} - b_{\lambda T}] J_{n-\lambda}(nMy/r_1) \qquad (4)$$

For the case of a helicopter rotor, the observed sound is the result of the continuous distributed loading along the span of the blade. Therefore the power spectral density of radiated sound is given by

$$P(\vec{x},n) = \lim_{T\to\infty} \frac{1}{T} \int_0^T dt \int_{\eta} \int_{\eta'} C_n(\vec{x},\eta)\ C_n^*(\vec{x},\eta')\, d\eta\, d\eta' \qquad (5)$$

where C_n^* is the complex conjugate of C_n. Substituting for C_n from equation (4) and noting that the summation and the integral remains unchanged, provided the argument of the Bessels functions $M_t y/r_1$ is constant, result in the following Mach number scaling law to predict the rotational noise of n^{th} harmonics

$$P(\vec{n}_2, n, M_t) = P(\vec{x}_1, n, M_{t_1}) \left\{\frac{M_{t_2}}{M_{t_1}}\right\}^6 \left\{\frac{c_2}{c_1}\right\}^2 \left\{\frac{r_1}{r_2}\right\}^2 \left\{\frac{\sin \alpha_2}{\sin \alpha_1}\right\}^2 \quad (6)$$

where $\sin \alpha = x/r_1$.

In case of forward flight, r_1 should be replaced by $r_1(1-M_{or})$ where M_{or} is the component of forward flight Mach number in the direction of observer. Following similar procedure cited above, we obtain

$$P(\vec{x}_2,n,M_{t2}) = P(\vec{x}_1,n,M_{t_1}) \left\{\frac{M_{t_2}}{M_{t_1}}\right\}^6 \left\{\frac{c_2}{c_1}\right\}^2 \left\{\frac{r_1}{r_2}\right\}^2 \left\{\frac{\sin\alpha_2}{\sin\alpha_1}\right\}^2$$

$$\left\{\frac{1 + \mu_1 M_{t_1} \cos\alpha_1, \cos\phi_1}{1 + \mu_2 M_{t_2} \cos\alpha_2 \quad \cos\phi_2}\right\}^4 \quad (7)$$

A special case arises when the observer is directly above the axis of the rotor. For this case, $y/r_1 = b$, and the entire sound field will be due to only one loading harmonic $n = \lambda$. Hence both equations (6) and (7) reduce to

$$P(\vec{x}_2, n, M_{t2}) = P(\vec{x}_1, n, M_{t_1}) \left\{\frac{M_{t_2}}{M_{t_1}}\right\}^6 \left\{\frac{c_2}{c_1}\right\}^2 \left\{\frac{r_1}{r_2}\right\}^2 \quad (8)$$

which is the conventional sixth power Mach number scaling law.

To verify the validity of the Mach number scaling formula, a detailed experimental program was completed in the M.I.T. anechoic wind tunnel facility. A periodic sampling technique which is described above was used in determining the intensity of rotational harmonics.

In Figures 8 and 9 are shown the results of the Mach number scaling formula for lower and higher rotational harmonics of a two-bladed rotor on axis. The experimental results at a tip Mach number of 0.15 were used to predict the sound pressure levels at other Mach numbers. As can be seen from Figures 8 and 9, the theoretical Mach number scaling formula given by equation (8) yields better comparison with the experimentally obtained data for higher rotational harmonics. The discrepancy of the scaling formula for lower rotational harmonics is attributed to the fact that the measurements were made in the acoustic near field because of the physical limitations of the wind tunnel facility. In Figures 10 and 11 are shown the scaling results for the lower and higher harmonics of a two-bladed rotor off axis. Here the experimental results of the rotor operating at a tip Mach number of 0.15 and at an angle of 59° were used to predict the sound pressure levels at other Mach numbers.

Figure 12 depicts the directivity of rotational harmonics of a two-bladed rotor. The directivity data were obtained by positioning the micro-

phones at 10° intervals and using the periodic sampling technique. As can be seen from Figure 12, the directivity is dependent on the harmonic number and becomes all the more important for the off axis Mach number scaling law.

Mach Number Scaling of Low Frequency Broadband Noise

Since the broadband noise from rotors and propellers often appears to follow roughly a M_0^6 dependence, it is natural to postulate that unsteady, but random, forces on blades are responsible for its generation. Lowson and Ollerhead [13], Ffowcs Williams and Hawkings [14], and Morfey and Tanna [15] have theoretically related the radiated broadband acoustic spectrum from a single blade to the blade load spectrum without specifying how the loads are generated. Their results take no account of blade-to-blade correlations which might exist in practical applications. Lowson [16] proposed to account for this by postulating a frequency independent spatial correlation scale. Rotational harmonics are generated by the passage of blades through steady asymmetric velocity variations in the plane of the rotor. The low frequency broadband noise, on the other hand, is generated by passage of blades through a turbulent or a randomly varying velocity field. One essential difference between the harmonic loading and random loading is the bandwidth of excitation. The origin of turbulence, as related to its effects on broadband noise, in most cases seems rather inconsequential. It is mainly due to atmospheric inhomogeneities, but upstream obstructions such as fuselage and/or the wakes shed by the moving wing or blade might very well be the source of turbulence. A lifting rotor produces a mean downward velocity field which draws the atmospheric eddies through the rotor plane with a convecting velocity V_c. This random variation in "upwash" induces a random variation in the angle of incidence and hence a fluctuating blade load. As atmospheric turbulence contains a spectrum of wave number components, the resulting loading spectrum may affect the acoustic spectrum over the entire range of frequencies.

Many of the possible mechanisms for broadband noise generation by a single stationary airfoil in a moving stream have been the subject of various investigators. The nonuniform velocity field associated with turbulence leads to an unsteady blade load that is dipole in nature. Amiet [17] studied the resulting noise pattern by using the nonstationary airfoil theory of Sears [18]. However, in the case of rotating blades, the problem becomes more complex. The very fact that the blades are rotating can be looked at in terms of Doppler shifts in frequency. The presence or absence of a blade at various spatial locations may in fact be interpreted as temporal variations seen in the observer coordinates. Thus, a wide range of frequencies is generated at a single blade passage harmonic $mB\Omega$.

A hovering or low forward speed rotor may modify any ingested turbulence due to distortion of fluid elements drawn into the rotor plane. The turbulent eddies, in general, are elongated in the direction of convection velocity and often are chopped several times as they pass through the plane of the rotor. Figure 13 depicts the rotor geometry showing the definitions of symbols and convection velocity of a turbulent eddy. The time interval Δt for equally

spaced blades to pass a fixed point on the rotor plane is given by:

$$\Delta t = \frac{2\pi R_0/B}{2\pi\Omega R_0} = \frac{1}{\Omega B} \tag{9}$$

On the other hand, the time scale for an eddy of wavelength λ_ξ to be convected past a given point in the rotor plane is given by

$$t_\xi = \frac{\lambda_\xi}{V_c} \tag{10}$$

Here the eddy wavelength λ_ξ is given by $2\pi\Lambda/\xi$. Thus the ratio of blade passage time to eddy convection time is

$$\frac{\Delta t}{t_\xi} = \frac{1}{2\pi}\,\frac{\xi V_c}{B\Lambda\Omega} \tag{11}$$

Homicz and George [19] gave an expression for the far field radiated sound resulting from loading due to a turbulent upwash and predicted a smooth spectrum at frequencies beyond f_0 which is

$$\frac{f_0}{\Omega} = \frac{B(1 + M_0/M_c)}{2(1 - M_0\cos\phi)} \tag{12}$$

Also, the values of turbulent wave numbers ξ which make significant contributions to the acoustic spectrum at a given frequency f are given by

$$\frac{(f/\Omega)(1 - M_0\cos\phi)}{(V_c/\Lambda\Omega)(1 + M_0/M_c)} < \xi < \frac{(f/\Omega)(1 + M_0\cos\phi)}{(V_c/\Lambda\Omega)} \tag{13}$$

Combining equations (7) and (8), the lower limit for ξ which makes significant contributions for frequencies $f >> f_0$ is obtained as

$$\xi_f > \frac{B\Lambda\Omega}{2V_c} \tag{14}$$

Using equation (6), this result may be interpreted as follows

$$\frac{\Delta t}{t_\xi} >> 1 \qquad \text{when } f >> f_0 \tag{15}$$

Thus, a turbulent eddy of length scale of about 1 meter will take the order of one second to be drawn through a rotor plane with a convection velocity of about 1 m/sec. Hence, for a two-bladed rotor at 10 Hz, about 10 blade passages will encounter parts of the same eddy. This results in a pronounced blade-to-blade correlation effect and leads to positive and negative interference between acoustic waves generated by blades. On the other hand, a turbulent

eddy of length scale of about 10 cm or less will completely pass through the plane of the rotor between consecutive blade passage. The resulting rapid modulation of high frequency blade loading implies wider side bands and hence the radiated sound spreads over a large part of the acoustic spectrum.

When there is no significant blade-to-blade correlation, the total radiation is given by simply adding the uncorrelated sound power spectral densities of each of the blades. The radiation of a single blade, approximated by a rotating point dipole, has been given by Ffowcs Williams and Hawkings [14] as

$$\langle S_{pp}(\vec{x},f)\rangle = \frac{f^2}{4\rho_0 C_0^3 r^2} \sum_{n=-\infty}^{\infty} D_r(\phi,\ f-n\Omega)\ J_n^2\left(\frac{fR_0\cos\phi}{c_0}\right) \tag{16}$$

where $D_r(\phi,f)$ is the power spectral density of the dipole strength in the direction of radiation. The dipole source field is a direct consequence of the unsteady forces acting on the airfoil surface and is related to the power spectral density of the unsteady lift as follows

$$D_r(\phi,f) = \Phi_{LL}(f)\ \sin^2\phi \tag{17}$$

Under the assumptions of stationary isotropic turbulence, the unsteady lift spectrum is directly related to the turbulence upwash spectrum and the aerodynamic transfer function. For frequencies f >>0, the one sided power spectral density is given by

$$\Phi_{LL}(f) = \frac{2}{Q} \int_{-\infty}^{\infty}\int_{-\infty}^{\infty} dk_y dk_z \Phi_{ww}(f/Q,\ k_y,\ k_z)\ |K(f/Q,\ k_y)|^2 \tag{18}$$

Since the measured spectrum of turbulence was close to the one predicted by von Karman's interpolation formula, the corresponding two dimensional spectrum of the vertical component is given by

$$\Phi_{ww}(k_x,\ k_y) = 0.4548\ \bar{w}^2\Lambda_f^4 \frac{k_x^2 + k_y^2}{[1 + 1.793\Lambda_f^2\ (k_x^2 + k_y^2)]^{7/3}} \tag{19}$$

The aerodynamic transfer function used in equation (18) was given by Osborne [20] as follows

$$|K(k_x,\ k_y)| = \frac{1}{2}\rho_0 Qbc\ \frac{\frac{2\pi}{\beta}\left[J_0^2\left(\frac{M_0^2\pi c}{\beta^2}\ k_T\right) + J_1^2\left(\frac{M_0^2\pi c}{\beta^2}\ k_T\right)\right]^{1/2}}{\left[1 + \frac{2\pi^2 c}{\beta^2}\ k_T\right]^{1/2}} \tag{20}$$

where $k_T = (k_x^2 + k_y^2)^{1/2}$

Substitution of equations (20) and (19) in (18) and then in equation (16) yields the expression for the intensity and spectrum of low frequency broadband noise as follows

$$\langle S_{pp}(\vec{x},f)\rangle = \frac{f^2\sin^2\phi}{2Qc_0^3r^2\rho_0(1+bf/Q)} \sum_{n=-\infty}^{\infty} D_r(f-n\Omega)J_n^2\left(\frac{fR_0\sin\phi}{c_0}\right) \tag{21}$$

where

$$D_r(f) = \frac{\pi^2\rho^2Q^2b^2c^2(0.4548)}{\beta^2}\,\bar{w}^2\,\Lambda_f^4$$

$$\int_0^{\infty} \frac{dk_y[(f/Q)^2+k_y^2][J_0^2(\frac{M_0^2\pi c}{\beta^2}\sqrt{(f/Q)^2+k_y^2})+J_1^2(\frac{M_0^2\pi c}{\beta^2}\sqrt{(f/Q)^2+k_y^2})]}{[1+\frac{2\pi^2c}{\beta^2}\sqrt{(f/Q)^2+k_y^2}][1+1.793\Lambda_f^2\{(f/Q)^2+k_y^2\}]^{7/3}} \tag{22}$$

Numerical calculations were performed for the measured values of turbulence intensities and integral scales for various advance ratios and tip Mach numbers. The note that the above analysis of low frequency broad band noise follows closely that of Homicz and George [19] and George and Kim [21].

Figure 14 and Figure 15 compare the predicted and the measured narrow band spectra for the large and the small turbulence generating grids, respectively. The acoustic spectra obtained are corrected for the experimentally obtained two-bladed rotor results with a 6% bandwidth analysis by adding 3 dB to the entire spectrum. The experimental plot is deliberately terminated around 3000 Hz, beyond which is assumed to be the region of high frequency broadband noise. As can be seen from Figures 14 and 15, the agreement between measured and the predicted spectra is better for the larger grid with an integral scale of 8.5 cm. The results of the rotor operating with no upstream turbulence generator are not plotted because at these frequencies the background noise was comparable to the intensity of the low frequency broadband noise. In Figure 16 is plotted the effect of advance ratio on the predicted peak intensity of the low frequency broadband noise. As can be seen from the figure, a doubling of advance ratio results in an increase of peak sound pressure level of about 8 dB. This result is not surprising because of the increased r.m.s. value of turbulence in the tunnel with increasing forward speed. Since the theory predicts a 6 dB increase in doubling the turbulence velocity, only the remainder must be thought of as the true influence of advance ratio. Caution must be exercised in comparing these results with those of full scale rotors since increase in advance ratio does not significantly change the turbulence encounter.

In Figure 17 is plotted the peak intensity of the low frequency broadband noise as a function of the relative tip velocity. In plotting this figure, the effect of the increase in the r.m.s. turbulence levels is removed by taking out 20 log $\bar{w}_2/\bar{w}_1$ from the predicted sound pressure levels. The levels are normalized with respect to the predicted sound pressure level at a velocity of 34.8 m/sec. Also plotted in the figure are measured sound pressure levels for a two-bladed rotor. As can be seen from the figure, a 12 dB increase per doubling velocity seems to fit the predicted and the measured data very well. Including the effect of increase in r.m.s. turbulence levels would result in the conventional V_t^6 power law. The location of the peak intensity in the frequency domain increases with increase in tip velocities.

In Figure 18 are plotted the predicted sound pressure levels as a function of the turbulence integral scale for a fixed value of the tip velocity of 80.8 m/sec. Once again, we observe that the location of the peak intensity in the frequency domain decreases with an increase in the integral scale of turbulence. In Figure 19 is plotted the peak intensity of LFBN as a function of the longitudinal integral scale Λ_f of turbulence. Here, the effect of the rotational velocity and the increase in turbulence intensity are removed. As can be seen from the figure, the peak intensity is a very weak function of Λ_f. This weak dependence can be readily explained by an examination of equation (22) For relatively large values of frequency, we may approximate the denominator of equation (22) as

$$\left[1 + \frac{2\pi^2 c}{\beta^2}\sqrt{(f/Q)^2 + k_y^2}\right]\left[1.793\,\Lambda_f^2\,\{(f/Q)^2 + k_y^2\}\right]^{7/3}$$

Since the integral is independent of Λ_f, we readily obtain a scaling factor based on Λ_f as

$$D_r(f) \sim \Lambda_f^{-2/3}$$

which would result in a reduction of approximately 2 dB per doubling the integral scale.

An examination of Figures 14 through 19 suggests that the location of the peak intensity of low frequency broadband noise in the frequency domain can be scaled with reference to a Strouhal number defined as follows

$$S = \frac{f_p \Lambda_f}{V_t} \tag{23}$$

In Figure 20 are plotted the spectra of sound pressure levels for various Mach numbers and size scales of turbulence. It is interesting to see how the entire data collapse to a single curve defining a normalized acoustic spectra for the model rotor turbulence interaction noise as a function of the non-dimensionalized Strouhal frequency. The peak intensity appears at a frequency corresponding to a Strouhal number of about 1.5.

Mach Number Scaling of High Frequency Broadband Noise

In the preceeding section we discussed the possible mechanisms of low frequency broadband noise radiation from rotating airfoils and arrived at an acceptable Strouhal frequency scaling to predict intensity and spectrum of such a radiation. It was observed that at high enough frequencies, this radiation decays approximately like f^{-2}. Therefore, in absence of any other mechanism of radiation, the intensity of rotor generated noise would be insignificant at frequencies well beyond the peak of low frequency broadband noise radiation. But, our experimentally obtained model data as well as the full scale rotor data of Leverton [4] do not exhibit such a decrease in the measured acoustic spectra. In fact, the evidence of existence of another mechanism which radiates efficiently over the frequency range well beyond low frequency broadband noise peak is overwhelming. In this section we shall discuss the possible mechanisms appropriate for such high frequency radiation.

As mentioned before, the broadband part of the rotor noise spectrum is attributed to the nonperiodic time dependent loads. These fluctuations in force may arise as a result of (i) free stream disturbances generating a fluctuating angle of incidence, (ii) a turbulent boundary layer on the surface of the airfoil, and (iii) a spanwise vorticity in the wake of the airfoil. These mechanisms, in general, interact through nonlinear fluid mechanical processes. However, under certain conditions, it is possible to consider them as being mutually independent.

The interaction of the turbulent boundary layer with the trailing edge of an airfoil imparts momentum fluctuations to the surrounding media and the total radiated spectrum may be divided into turbulent boundary layer dominated components and wake dominated components. Chanaud and Hayden [22] have shown that when the dimensions of the radiating surface are small compared to the acoustic wave length, the contributions of the turbulent boundary layer to the total acoustic intensity are usually negligible relative to the contributions from the inflow turbulence or wake. In the absence of significant inflow turbulence, the wake generated noise would dominate the high frequency regime of the acoustic spectra.

Several independent experiments by Hersh and Hayden [23], Paterson, Vogt, Fink, and Munch [24], and Clark [25] revealed that discrete tones are emitted from isolated airfoils under certain operating conditions. Over a wide range of Reynolds number based on the chord of the airfoil, the total radiated sound could be dominated by these discrete tones. Further, the frequencies of these tones appear to be a well defined function of free stream velocity and form an organized pattern. There is a considerable amount of difference of opinion regarding the Strouhal frequency scaling of these discrete tones. Hersh and Hayden [23] and Paterson, Vogt, Fink, and Munch [24] have all attributed the generation of these tones to the classical vortex shedding along the span of the airfoil. The shed vortices generate a periodic pressure fluctuation over the airfoil at that particular Strouhal frequency, resulting in a edge dipole radiation.

Lee [26] made measurements of the peak frequency location of the high frequency broadband noise of the present model rotor system operating at various tip speeds. Based on his measurements, he defined a Strouhal number

$$S = \frac{ft}{V_e}$$

where V_e was the rotational velocity measured at 75% of the blade span. His experimental results lead to a Strouhal number of about 1. Following Lee's [26] argument that there is a need for a frequency scaling based more on geometrical parameters of the system than on the fluid dynamical characteristics, we define a priori a frequency scaling law as follows

$$f = \frac{SV_t}{t} \tag{24}$$

Based on our experimental results, the validity of such a relationship will be demonstrated below.

If we assume the compactness of the source and that the shed vortices are correlated over a distance ΔL of the blade span, the instantaneous pressure fluctuation at the observer location is readily given by

$$\Delta p = -\frac{1}{4\pi c_0} \frac{\cos\theta}{r_1} \frac{\partial}{\partial \tau} p_i(\tau) \, (c\Delta L)$$

where p_i is the instantaneous pressure fluctuation on the airfoil surface due to shed vortices. Normalizing the pressure with respect to the blade sectional velocity and integrating the mean square of the pressure over the span of the blade lead to the amplitude scaling of the high frequency broadband noise.

$$S_{pp}(f) \simeq \frac{S^2 c^2 \rho_0^2 b \, V_t^6 \Delta L}{c_0^2 t^2 r_1^2} \left[1 + \frac{14}{3}\mu + \frac{42}{5}\mu^2\right] \tag{25}$$

where the frequency f is given by the equation (24). The effect of number of blades may be included by multiplying equation (25) by blade number, B.

Mugridge [27] and Clark [28] demonstrated experimentally that the correlation lengths over a stationary airfoil are directly proportional to the displacement thickness of the turbulent boundary layer. In the case of a rotating airfoil, the thickness of the boundary layer is influenced by the local Reynolds number as well as by the spanwise flow. Realistic estimates of correlation lengths for rotating airfoils are not presently available. However, since the mechanism is similar to that of a stationary airfoil, we assume for scaling purposes that the correlation length behaves in a manner similar to the boundary layer displacement thickness at a representative spanwise location. Since the displacement thickness for the turbulent boundary layer varies like $c/(R_e)^{0.2}$, the high frequency broadband noise levels vary like $V_t^{5.8}$.

To verify the validity of the Mach number scaling procedure developed in this section, a series of experiments were performed under various operating conditions of the model rotor. The experimental results indicated that the mean thrust generated by the rotor had little effect on the intensity and spectrum of high frequency broadband noise. The increase in number of blades increased the intensity of high frequency broadband noise in addition to broadening of the high frequency broadband noise'hump.' A 3 dB per doubling of blade number fitted the measured data very well. The advance ratio had a significant effect on the intensity of high frequency broadband noise without affecting its spectrum. A 8 dB per doubling the advance ratio showed good agreement with the experimental data.

In Figure 21 are plotted typical high frequency broadband noise spectra for various rotational speeds at constant advance ratio for a two-bladed rotor. As noted above, the advance ratio had no significant effect on the peak frequency location, and this justifies use of rotational tip velocity in equation (24) for Strouhal scaling of shed vortices. Figure 22 shows a plot of peak frequency as a function of the blade tip velocity. As can be seen from Figure 22, the peak frequency is directly proportional to the blade tip velocity with a proportionality constant of 16.5. At higher tip speeds, the high frequency broadband noise is spread over a narrow range of frequencies and hence there is some scatter in the measured data. Using maximum blade thickness in equation (24), the resulting Strouhal frequency is 1.08. Although a wake characteristic length such as displacement of momentum thickness should be the appropriate length scale to be used, a simple relationship based on the geometrical parameter may be very useful in practical applications.

In Figure 23, an estimate of the peak sound pressure levels calculated using the measured values of a two-bladed rotor operating at 550 rpm as a base is plotted. The three-bladed rotor data are normalized with respect to the two-bladed rotor data by taking out 10 log B_2/B_1 from measured sound pressure levels. As can be seen from Figure 22, the prediction scheme presented herein gives good correlations with the measured two-blade and three-blade data except at very low rotational velocities. It was observed that at these low velocities, corresponding to a rotational speed of 300 and 400 rpm, the measured high frequency broadband noise spectra showed intense peaks. This probably is due to a fairly laminar flow on both sides of the airfoil resulting in more intense shedding of vortices. The peak intensity decreased slightly as we increased the rotational velocity to about 500 rpm, and then started increasing according to the postulated power law.

The effect of free stream turbulence, in general, is to decrease the intensity of high frequency broadband noise. In Figure 24 is shown the effect of turbulence on the 6% bandwidth spectrum of a two-bladed rotor operating at 672 rpm. One obvious reason for the reduction in the intensity of high frequency broadband noise is the premature transition of the laminar boundary layer on the blade surface. Evans and Horlock [29] studied the effect of free stream turbulence on a developing boundary layer and concluded that the displacement thickness of the boundary layer decreased with increasing free

stream turbulence intensity. In Figure 25 are depicted the computed and measured intensities of high frequency broadband noise as a function of turbulence in the free stream. From Figure 25 it is evident that the influence of turbulence on the intensity of high frequency broadband noise is indeed significant.

CONCLUSIONS

The objective of this study has been to arrive at suitable velocity dependent factors to predict the various noise components of a model helicopter rotor. To this end, we have performed a series of experiments at the M.I.T. anechoic wind tunnel facility. The rotational and the broadband noise components were isolated and studied independently. An analysis based on existing theoretical modelling of unsteady aerodynamics has been presented and the computed results have been compared with the measured data. In this section, based on our analysis and measured data, we have proposed the appropriate scaling laws governing the radiation of various components of model rotor noise.

It is postulated that the rotational noise from model rotors is a direct consequence of steady and unsteady loading harmonics and the broadband noise may further be classified into low frequency and high frequency components because of the inherent differences in their causative mechanisms. The low frequency broadband noise is attributed to the interaction of ingested turbulence with the rotor blades. The high frequency broadband noise is associated with the periodic vortex shedding from the rotating airfoils.

Analytical expressions were developed to determine the spectral content of the rotational noise components using existing theories of radiation from rotating dipole sources. An order of magnitude study indicated that the contribution of force derivative terms outweighs the contributions of force and thickness terms for tip Mach numbers of 0.6 or less. Such an approximation yielded simpler expressions for the complex Fourier coefficients of sound radiation from a rotating point source. The resulting Mach number scaling formula for rotational noise is as follows

$$SPL_2 = SPL_1 + 60 \log \frac{M_{t_2}}{M_{t_1}} + 20 \log \frac{c_2}{c_1} - 20 \log \frac{r_2}{r_1} + 20 \log \frac{\sin\alpha_2}{\sin\alpha_1} - 40 \log \left[\frac{1 + \mu_2 M_{t_2} \cos\alpha_2 \cos\phi_2}{1 + \mu_1 M_{t_1} \cos\alpha_1 \cos\phi_1} \right] \quad (26)$$

The location in the frequency domain is simply given by the blade passage harmonic, $nB\Omega$.

Theoretical analysis of the low frequency broadband noise was made exploiting the existing knowledge of unsteady thin airfoil theory and the characteristics of the inflow turbulence. Assumptions of isotropy and homogeneity of turbulence were made to make the analysis feasible. The measured spectrum of turbulence justified the validity of such assumptions. Further, it was observed that the measured turbulence spectra could easily be interpreted in terms of von Karman's interpolation formula. With the aid of this and the two dimensional Sears function, the unsteady lift acting on the airfoil was computed. The resulting acoustic intensity and spectra were dependent on the flow and rotational Mach numbers, intensity, and size scale of turbulence. The peak intensity of low frequency broadband noise was found to be varying with the Mach number according to a M_t^4 power law, and with r.m.s. values of turbulence velocity according to a $\bar{w}^2$ power law. The influence of size scale of turbulence on the peak intensity was found to be insignificant, approximately $\Lambda_f^{-0.33}$. However, the location of peak intensity in the frequency domain was found to be strongly dependent on the Mach number and the longitudinal scale of turbulence. To this end, we plotted the normalized acoustic intensity as a function of Strouhal frequency $f\Lambda_f/V$. It was observed that the peak intensity of LFBN occurred at a Strouhal number of about 1.5. With this, a scaling law can readily be proposed to evaluate the peak intensity of low frequency broadband noise. Under similar flow environ, the sound pressure level of a rotor system 2 in terms of a rotor system 1 will then be given as follows

$$SPL_2 = SPL_1 + 20 \log \frac{b_2 c_2}{b_1 c_1} + 10 \log \frac{\bar{w}_2^2}{\bar{w}_1^2} + 40 \log \frac{M_{t_2}}{M_{t_1}} + 20 \log \frac{\left|(1+\mu_2)^2 + (M_{c_2}/M_{t_2})^2\right|}{\left|(1+\mu_1)^2 + (M_{c_1}/M_{t_1})^2\right|} - 3.3 \log \frac{\Lambda_{f_2}}{\Lambda_{f_1}} - 20 \log \frac{r_2}{r_1} \quad (27)$$

The location of the peak intensity in the frequency domain is given by

$$f_{p_{1,2}} = \frac{1.5\ V_{1,2}}{\Lambda_{f_{1,2}}} \quad (28)$$

for respective rotor system.

To obtain a similar scaling procedure for high frequency broadband noise generated by a model rotor, we assumed that noise sources were acoustically compact and computed the instantaneous pressure due to an element of an airfoil where vortices are being shed. Extending experimentally obtained results for the spanwise correlation lengths for stationary airfoils to rotating airfoils

and assuming that the correlation lengths vary like the displacement thickness of the boundary layer, it was observed that the peak intensity of high frequency broadband noise has a $V_t^{5.8}$ factor. An expression which scales the location of peak intensity in the frequency domain was obtained based on the rotor blade geometric parameters. The resulting scaling laws for peak intensity was found to be

$$SPL_2 = SPL_1 + 60 \log \frac{M_{t_2}}{M_{t_1}} + 20 \log \frac{c_2 t_1}{c_1 t_2} + 10 \log \frac{b_2}{b_1} - 20 \log \frac{r_2}{r_1} + 10 \log \frac{(\Delta L)_2}{(\Delta L)_1} + 10 \log \left\{ \left[1 + \frac{14}{3} \mu_2 + \frac{42}{5} \mu_2^2 \right] \Big/ \left[1 + \frac{14}{3} \mu_1 + \frac{42}{5} \mu_1 \right] \right\} \quad (29)$$

and the peak frequency was found to be given by

$$f_{p_{1,2}} = 1.08 \, V_{t_{1,2}} \Big/ t_{1,2} \quad (30)$$

for the respective rotor systems. The effects of intensity and size scale of turbulence were less obvious in the study of high frequency broadband noise. One of the effects of free stream turbulence is to alter the correlation lengths of shed vortices. To this end, we used an existing integral boundary layer calculation to predict the turbulent boundary layers developing in a turbulent free stream. The results indicated that increase in the intensity of free stream turbulence in general would tend to decrease the correlation length, thus resulting in reducing the intensity of high frequency broadband noise.

The scaling laws obtained for the intensities of rotational noise components were experimentally verified over a range of operating conditions. The measured data showed general agreement with the scaling procedure except at low rotational harmonies. It is believed that the geometric and acoustic near field effects might have caused some ambiguity in the measured rotor noise spectra at very low frequencies. The low frequency broadband noise prediction procedures were experimentally verified under various operating conditions of the rotor and varying intensity and size scale of turbulence. A comparison of predicted peak frequency and sound pressure levels with experimental data showed good agreement except for the case of effect of turbulence on the intensity of high frequency broadband noise. In this case, the data showed general agreement with the prediction technique, but the measured intensity levels were higher than the predicted levels. We further

add that improvements in modelling more of the fluid mechanical aspects of the flow field are desired to place this scaling procedure on a firmer basis.

Our efforts in modelling the rotational noise components of the model rotor and understanding the effects of free stream turbulence on the nature of high frequency and low frequency broadband noise components have been greatly benefited from the detailed experimental task performed by Lee [26]. The utility of our results for scaling of low frequency and high frequency broadband noise remains as demonstrated in the above comparison of predictions and data. The scaling procedures developed in this study may be considered as a first order attempt in responding to the challenge of Mach number and Reynolds number scaling of full scale rotors.

REFERENCES

1. Gutin, L., "On the Sound Field of a Rotating Propeller," NACA TM 1195, 1948.

2. Cox, C.R., "Aerodynamic Sources of Rotor Noise," Journal of American Helicopter Society, 18, pp. 3-9, 1973.

3. Morfey, C.L., "Rotating Blades and Aerodynamic Sound," Journal of Sound and Vibration, 28, pp. 587-617, 1973.

4. Leverton, J.W., "The Noise Characteristics of a Large Clean Rotor," Journal of Sound and Vibration, 27, pp. 357-376, 1973.

5. Leverton, J.W. and Pollard, J.S., "A Comparison of Overall and Broadband Noise Characteristics of Full Scale and Model Helicopter Rotors," Journal of Sound and Vibration, 30, pp. 135-152, 1973.

6. Lowson, M.V., Whatmore, A.R., and Whitfield, C.E., "Source Mechanisms for Rotor Noise Radiation," NASA CR-2077, 1973.

7. Aravamudan, K.S. and Harris, W.L., "Experimental and Theoretical Studies on Model Helicopter Rotor Noise," M.I.T. Fluid Dynamics Research Laboratory Report 78-1, January 1978.

8. Lee, A., Harris, W.L. and Widnall, S.E., "A Study of Helicopter Rotor Rotational Noise," Journal of Aircraft, 14, 11, 1977, pp. 1126-1132.

9. Aravamudan, K.S., Lee, A., and Harris, W.L., "A Simplified Mach Number Scaling Formula for Helicopter Rotor Noise," Journal of Sound and Vibration, 57, 3, 1978.

10. Baines, W.D. and Peterson, E.G., "An Investigation of Flow Through Screens," Transactions of ASME, 73, pp. 467-480, 1951.

11. Harris, W.L. and Lee, A., "The Development of Experimental Techniques for the Study of Helicopter Rotor Noise," AIAA paper 75-455, AIAA 2nd Aeroacoustics Conference, Hampton, Virginia, March 24-26, 1975.

12. Hawkings, D.L. and Lowson, M.V., "Noise of High Speed Rotors," AIAA paper 75-450, AIAA 2nd Aeroacoustics Conference, Hampton, Virginia March 24-26, 1975.

13. Lowson, M.V. and Ollerhead, J.B., "A Theoretical Study of Helicopter Rotor Noise," Journal of Sound and Vibration, 9, pp. 197-222, 1969 (also Wyle Research Staff Report WR 68-9, 1968).

14. Ffowcs Williams, J.E. and Hawkings, D.L., "Theory Relating to the Noise of Rotating Machinery," Journal of Sound and Vibration, 10, pp. 10-21, 1969.

15. Morfey, C.L. and Tanna, H.K., "Sound Radiation from a Point Source in Circular Motion," Journal of Sound and Vibration, 15, pp. 325-351, 1971.

16. Lowson, M.V., "Rotor Noise Radiation in Non-Uniform Flow," Proceedings of the Symposium on Aerodynamic Noise, Loughborough University, Paper D2, 1970.

17. Amiet, R.K., "Acoustic Radiation from an Airfoil in a Turbulent Stream," Journal of Sound and Vibration, 41, pp. 407-420, 1975.

18. Sears, W.R., "Some Aspects of Non-Stationary Airfoil Theory and Its Applications," Journal of Aeronautical Sciences, 8, pp.104-108,1941.

19. Homicz, G.F. and George, A.R., "Broadband and Discrete Frequency Radiation from Subsonic Rotors," Journal of Sound and Vibration, 36, pp. 151-177, 1974.

20. Osborne, C., "Unsteady Thin Airfoil Theory," AIAA Journal, 11, pp. 205-209, 1973.

21. George, A.R. and Kim, Y.N., "High Frequency Broadband Rotor Noise," AIAA Journal, 15, 4, pp. 538-546, 1977.

22. Chanaud, R.C. and Hayden, R.E., "Edge Sound Produced by Two Turbulent Wall Jets," Paper FF-11, Spring Meeting of Acoustical Society of America, Atlantic City, New Jersey, 1970.

23. Hersh, S. and Hayden, R.E., "Aerodynamic Sound Radiation from Lifting Surfaces with or without Leading Edge Serrations," NASA CR-114370, 1971.

24. Paterson, R.W., Vogt, P.G., Fink, M.R., and Munch, C.L., "Vortex shedding Noise from Isolated Airfoils," Journal of Aircraft, 10, pp.296-302, 1973.

25. Clark, L.T., "The Radiation of Sound from an Airfoil Immersed in Laminar Flow," Journal of Engineering for Power, 13, Ser. A, pp.366-376, 1971.

26. Lee, A., "Theoretical and Experimental Study of Helicopter Rotor Noise," PhD. Thesis, Dept. of Aeronautics and Astronautics, M.I.T., 1975.

27. Mugridge, B.D., "Turbulent Boundary Layers and Surface Pressure Fluctuations on Two Dimensional Aerofoils," Journal of Sound and Vibration, 18, pp. 475-486, 1971.

28. Clark, L.T., "A Prediction Model for Wake Related Sound Generation," Ph.D. Thesis, University of Washington, 1973.

29. Evans, R.I. and Horlock, J.H., "Calculation of the Development of Turbulent Boundary Layers with a Turbulent Free Stream," ASME Paper 74-FE-24, 1974.

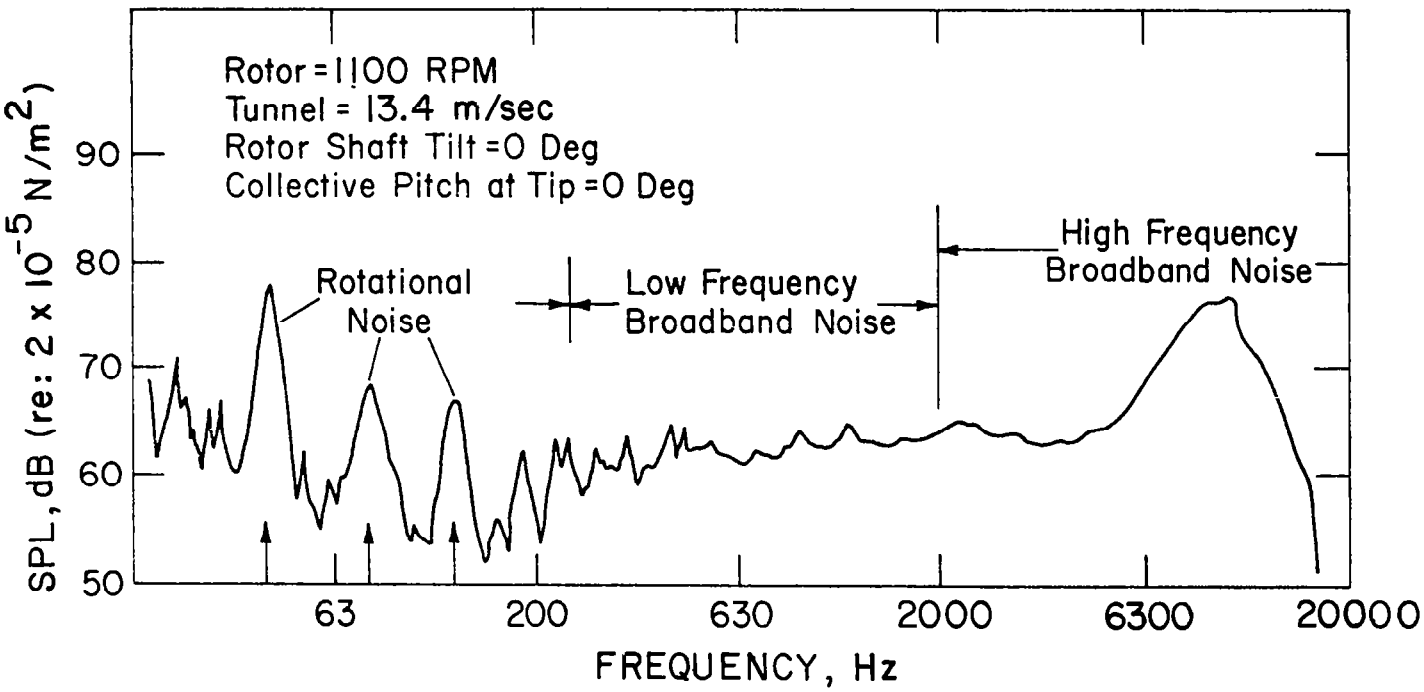

Figure 1.- 6% bandwidth spectrum of model rotor noise.

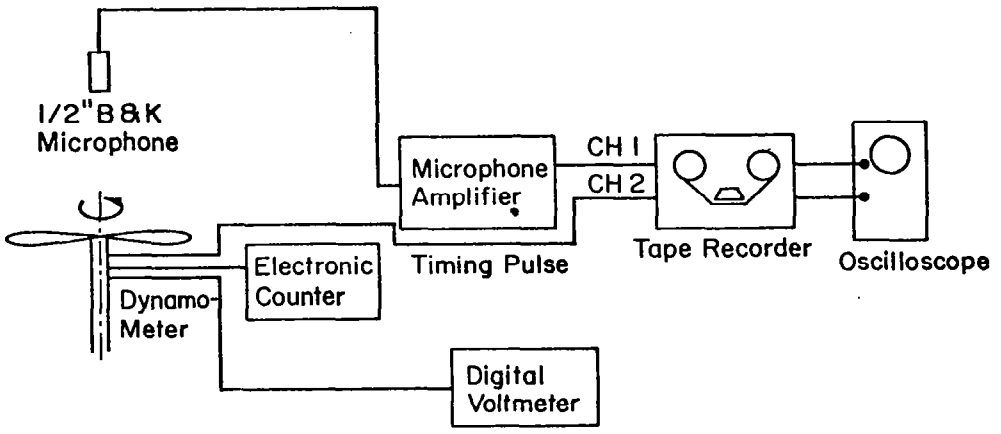

SCHEMATIC OF INSTRUMENTATION FOR ACQUISITION OF ACOUSTIC DATA

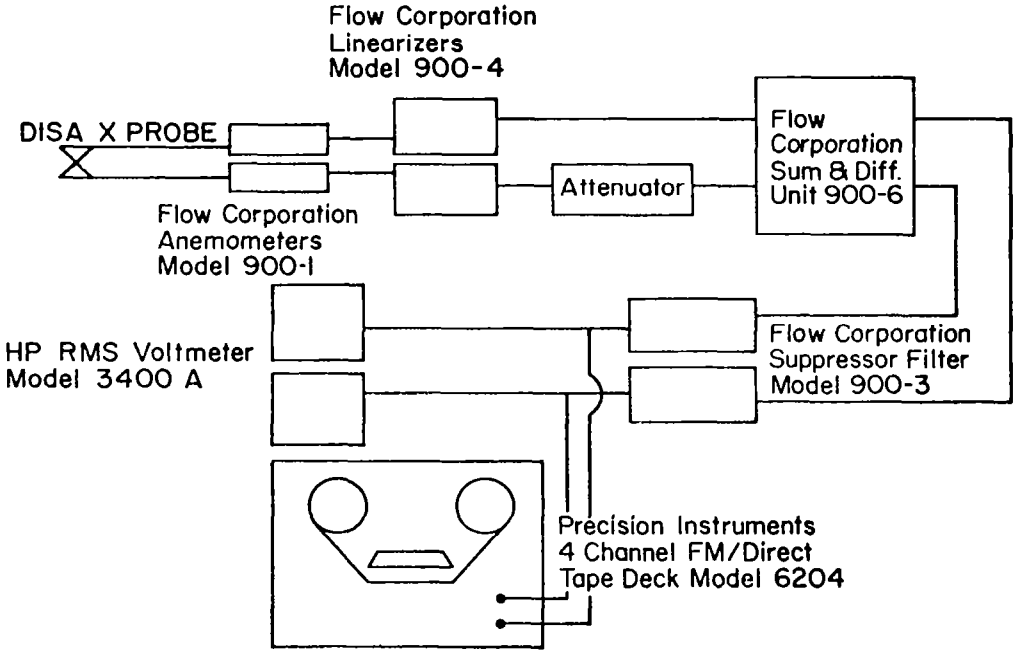

SCHEMATIC OF INSTRUMENTATION FOR ACQUIRING TURBULENCE DATA

Figure 2.- Schematic of instrumentation for acquiring turbulence data. (1/2 in. = 1.27 cm.)

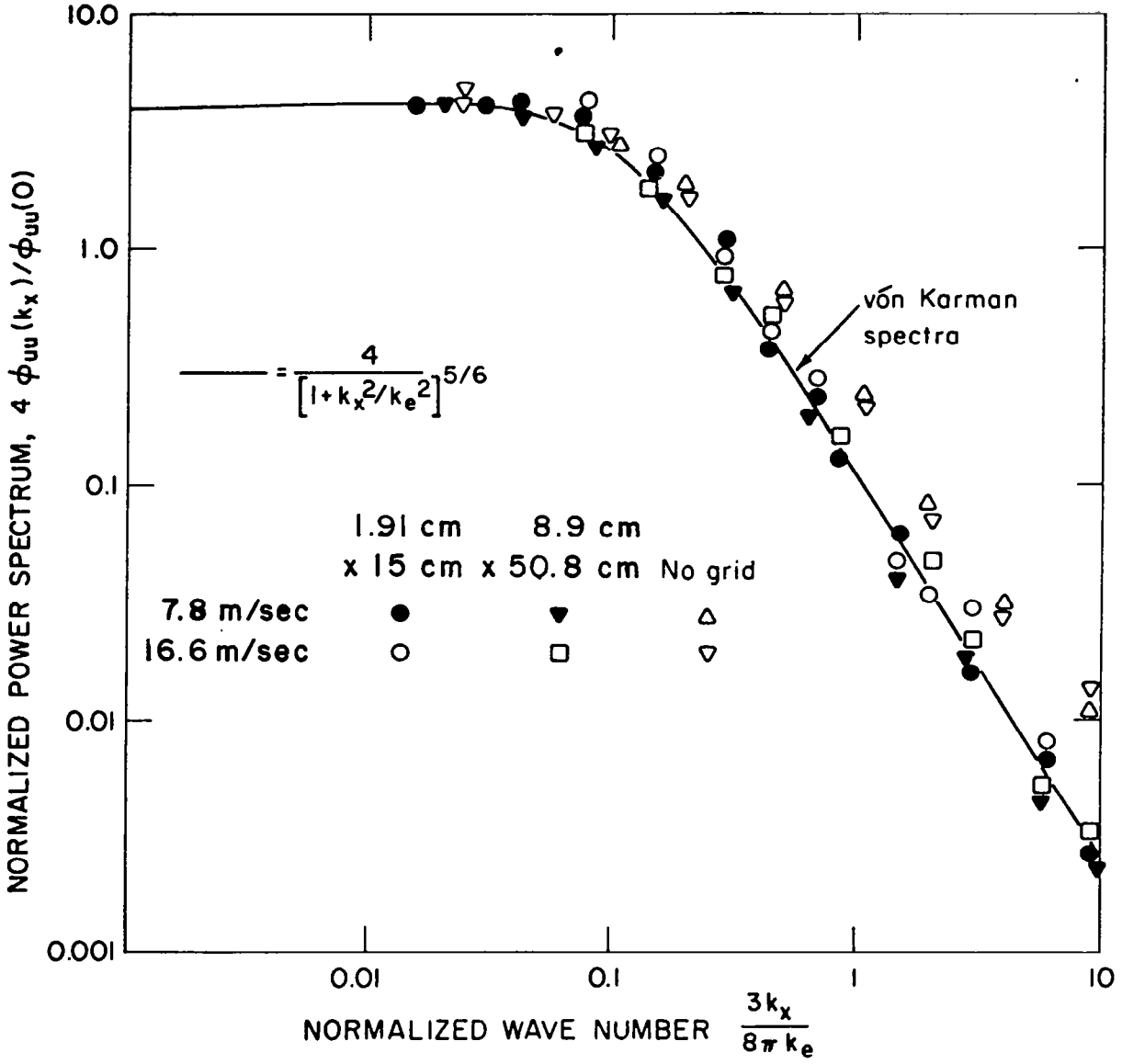

Figure 3.- One dimensional spectrum of axial component of grid turbulence.

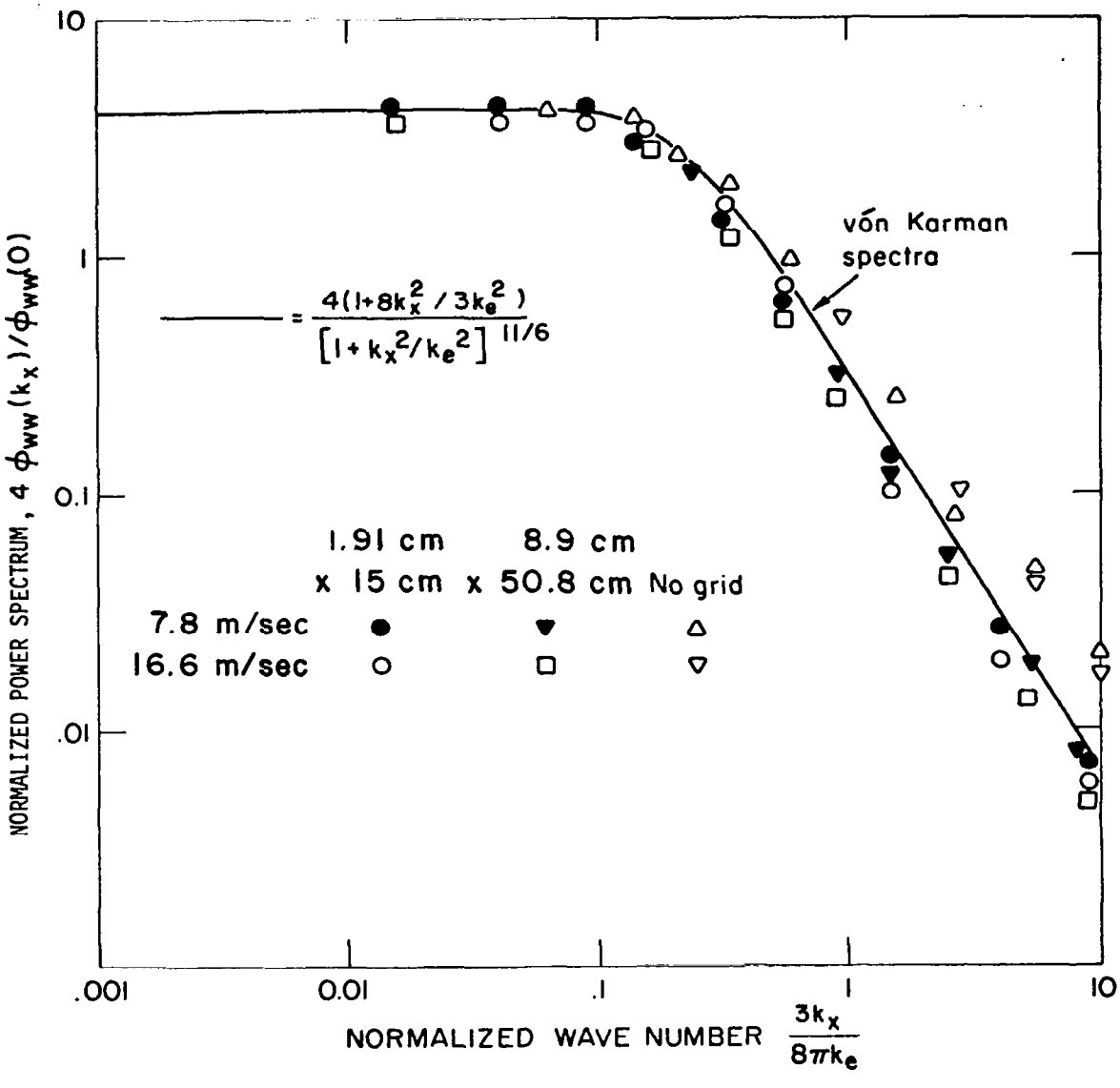

Figure 4.- One dimensional spectrum of vertical component of grid turbulence.

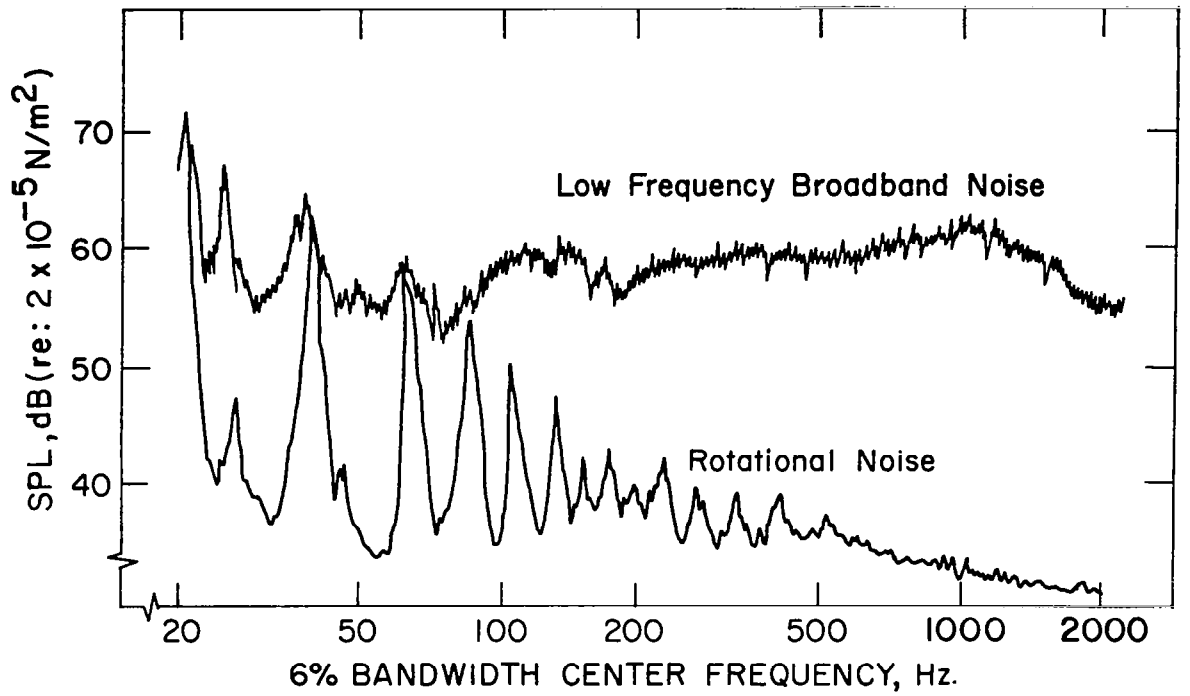

Figure 5.- Comparison of rotational noise and low frequency broadband noise at high frequencies for 1.91 cm × 15 cm turbulence grid; B = 2; Ω = 672 rpm; U_o = 13.4 m/sec.

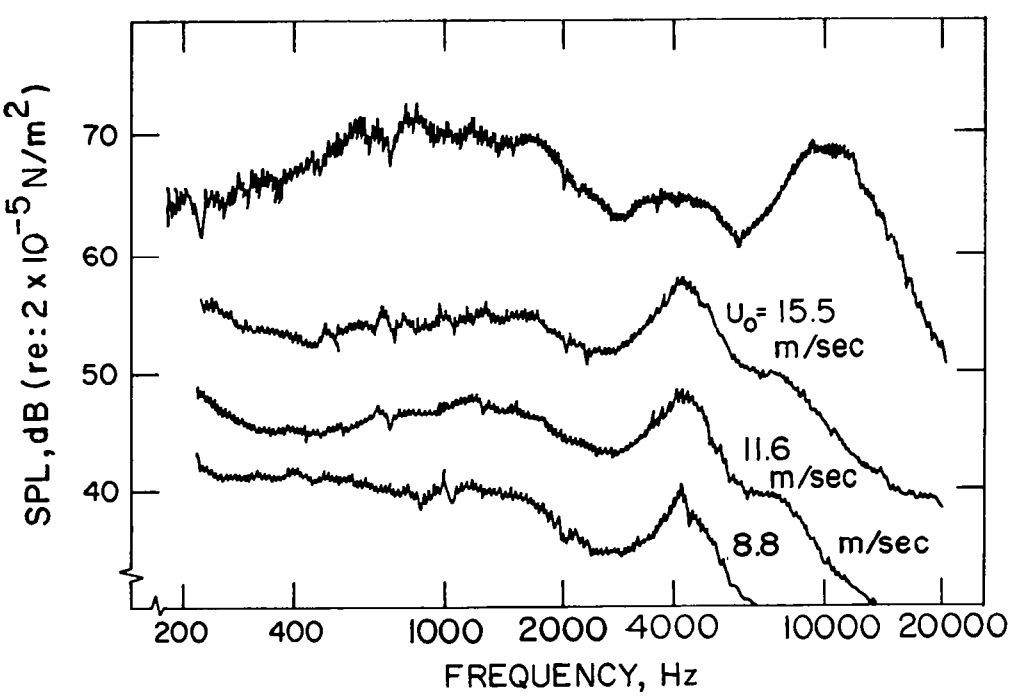

Figure 6.- 6% bandwidth background spectra at various tunnel speeds for 1.91 cm × 15 cm turbulence grid. Top curve: Rotor generated noise for B = 3; Ω = 1000 rpm; and U_o = 15.5 m/sec.

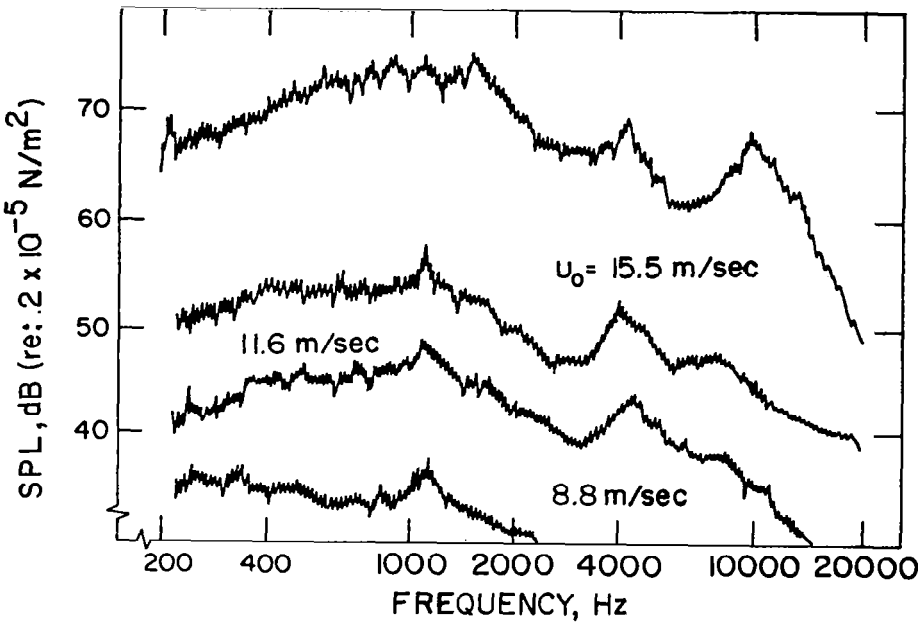

Figure 7.- 6% bandwidth background spectra at various tunnel speeds for 8.9 cm × 50.8 cm turbulence grid. Top curve: Rotor generated noise for B = 3; Ω = 1000 rpm; and U_o = 15.5 m/sec.

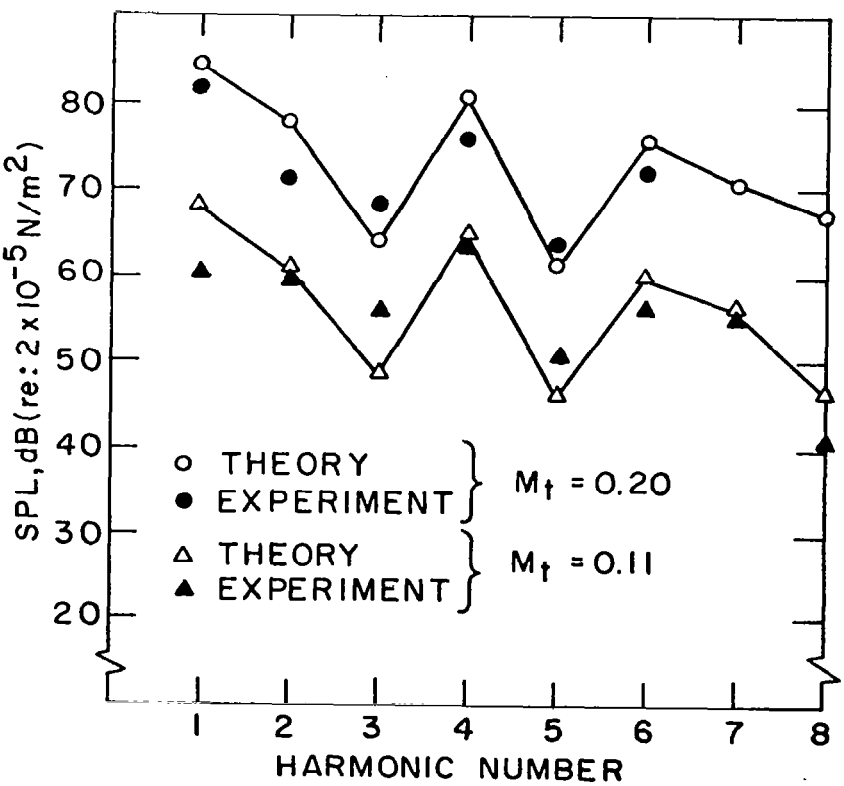

Figure 8.- Mach number scaling for lower harmonics of a two-bladed rotor on axis.

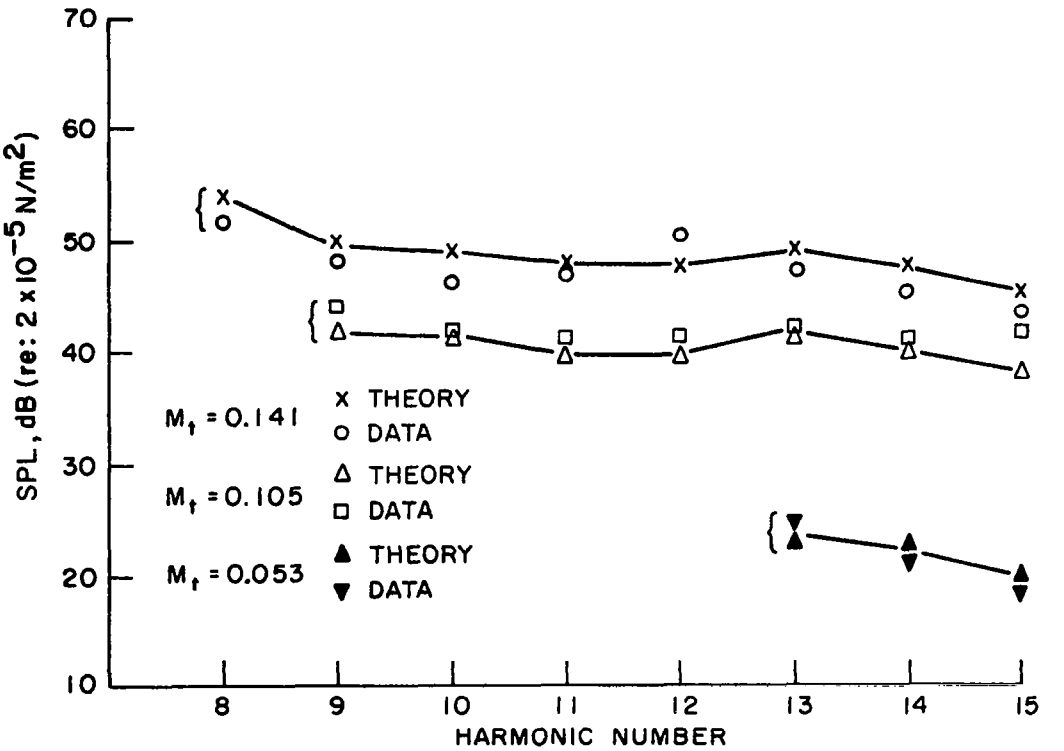

Figure 9.- Mach number scaling for higher harmonics of a two-bladed rotor on axis.

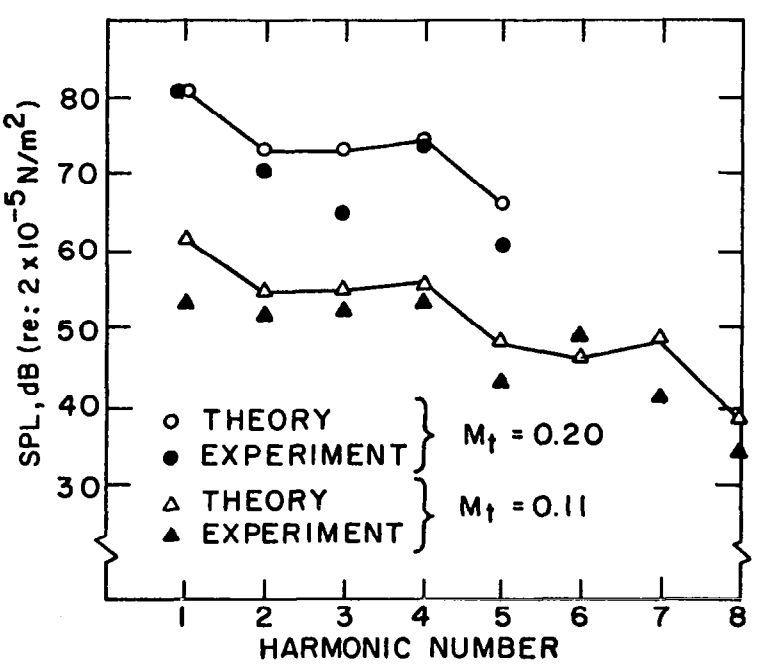

Figure 10.- Mach number scaling for lower harmonics of a two-bladed rotor off axis.

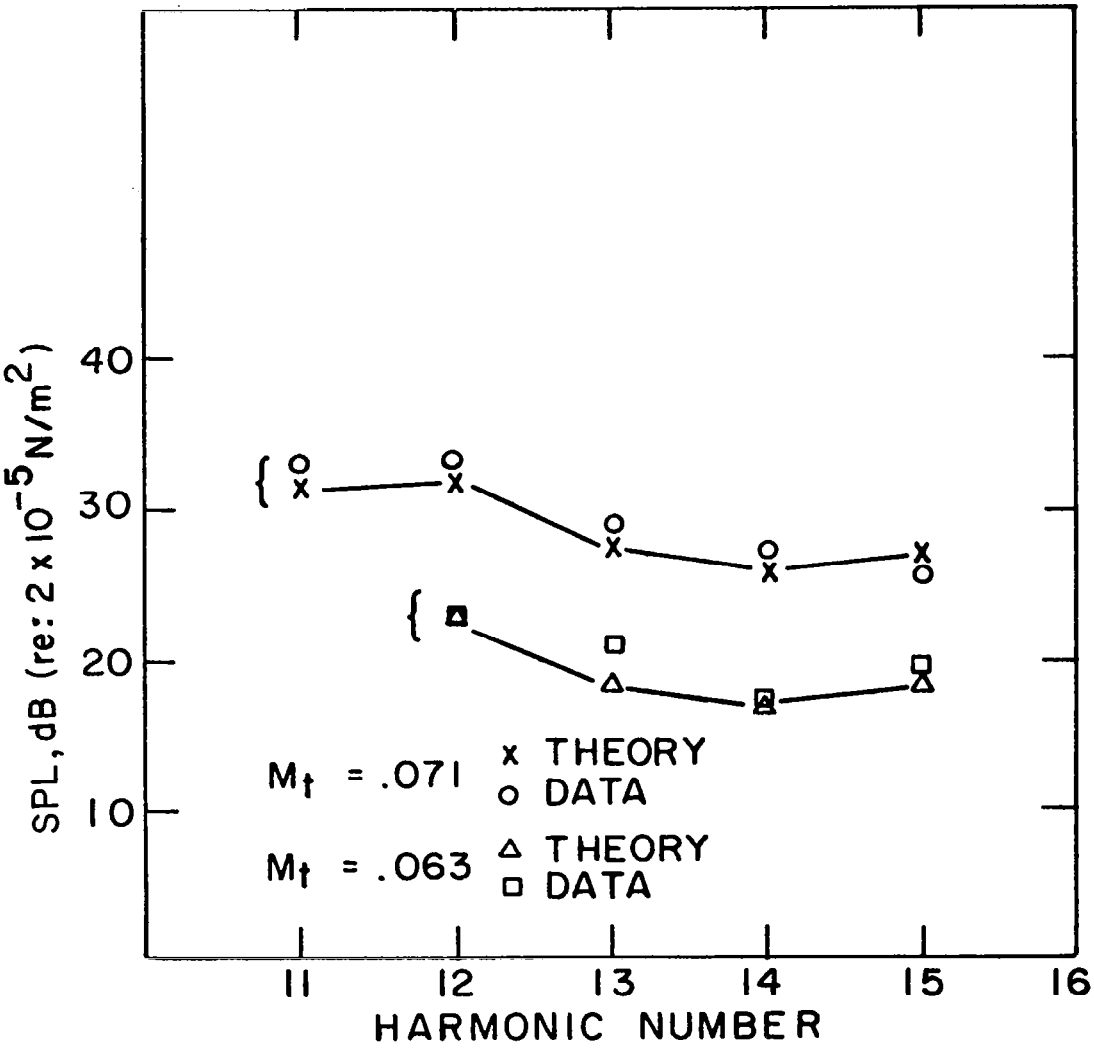

Figure 11.- Mach number scaling for higher harmonics of a two-bladed rotor off axis.

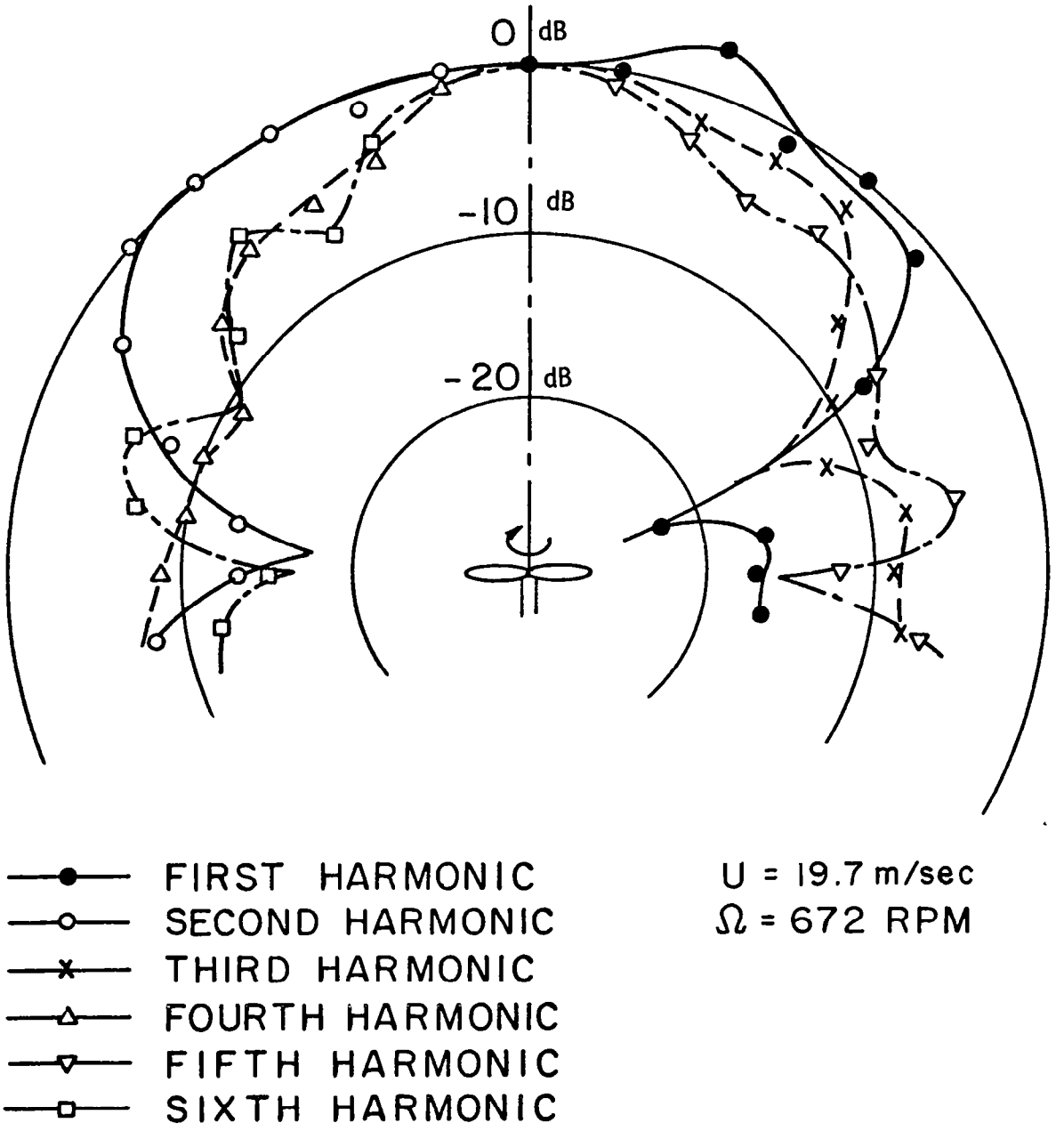

Figure 12.- Directivity of rotational harmonics of a two-bladed rotor.

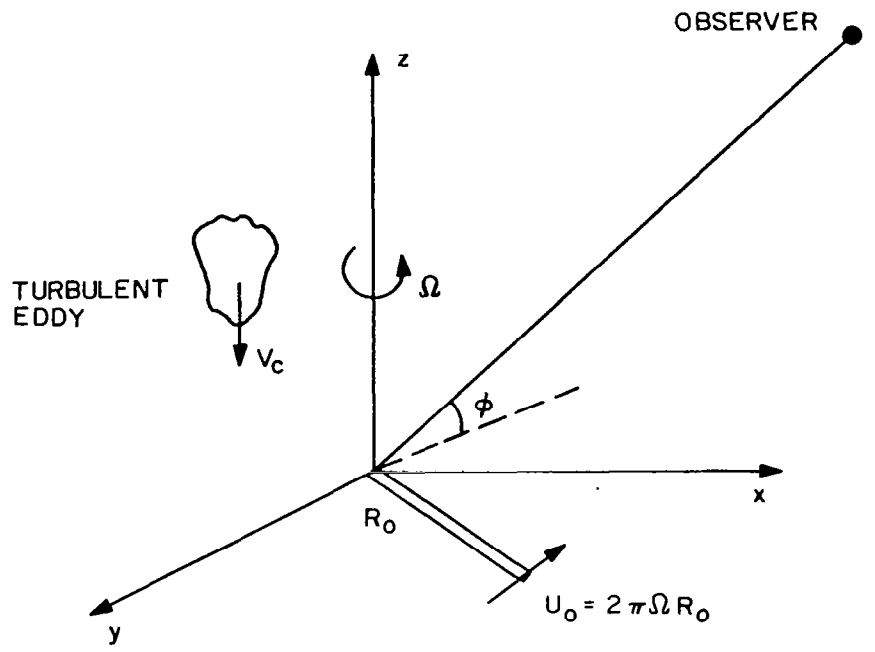

Figure 13.- Rotor geometry and coordinate system used.

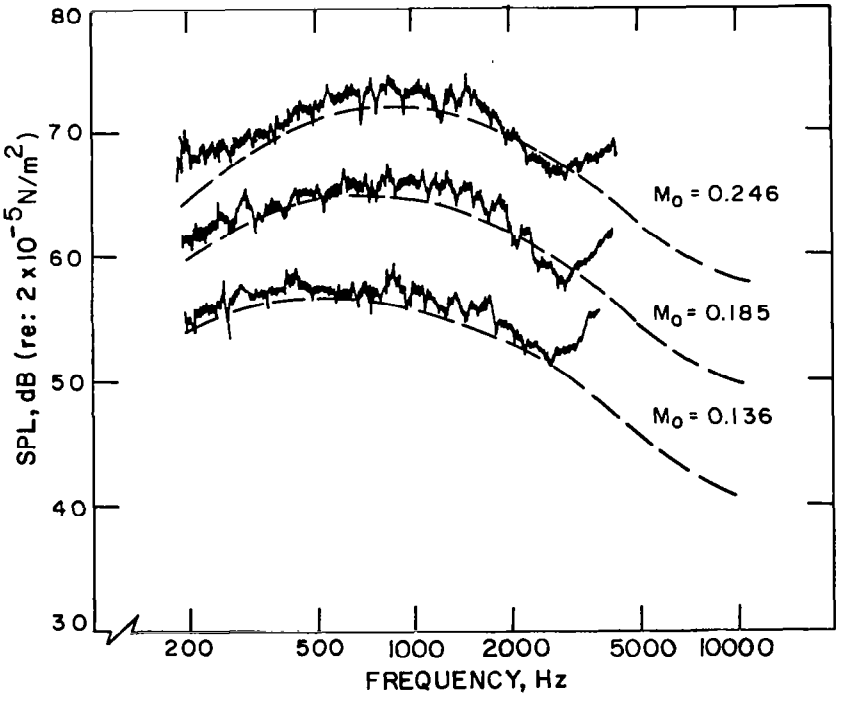

Figure 14.- Effect of Mach number on predicted and measured low frequency broadband noise for the larger grid with a Λ_f = 12.82 cm.

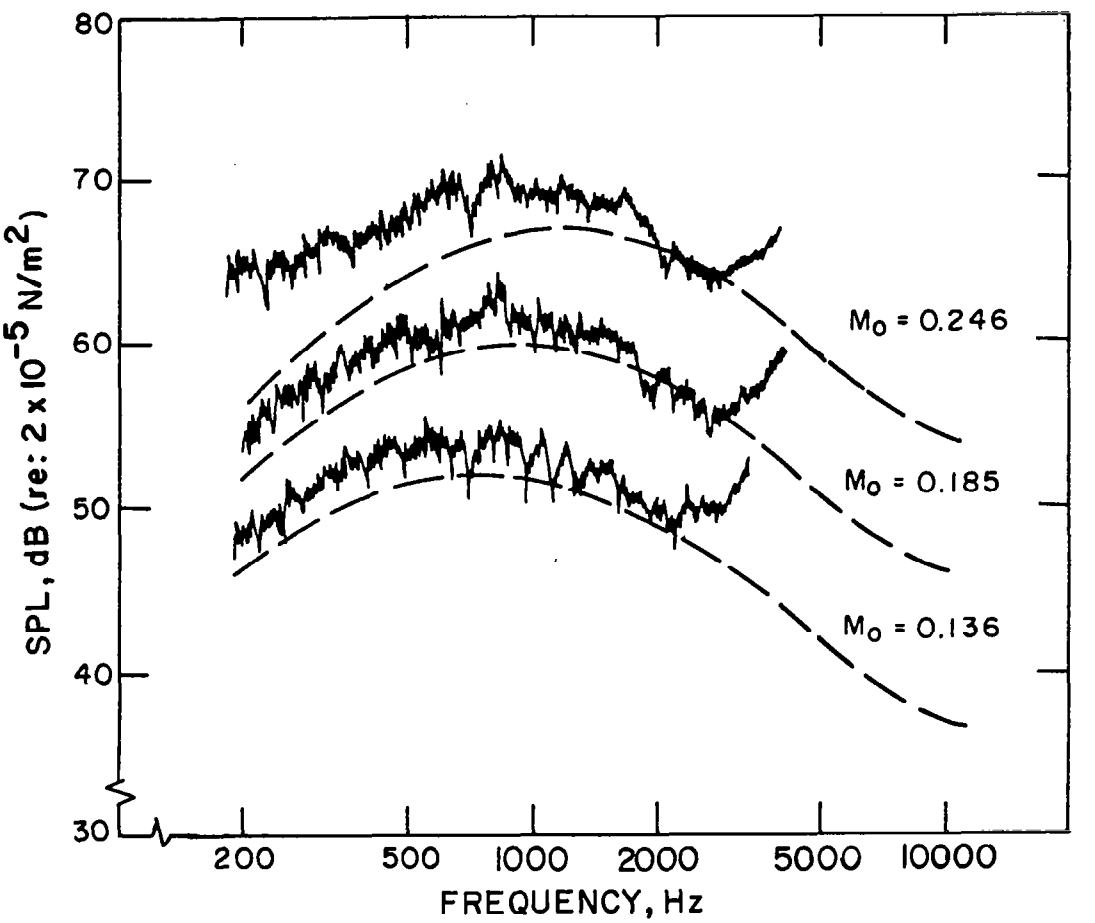

Figure 15.- Effect of Mach number on predicted and measured low frequency broadband noise for the smaller grid with a Λ_f = 8.46 cm.

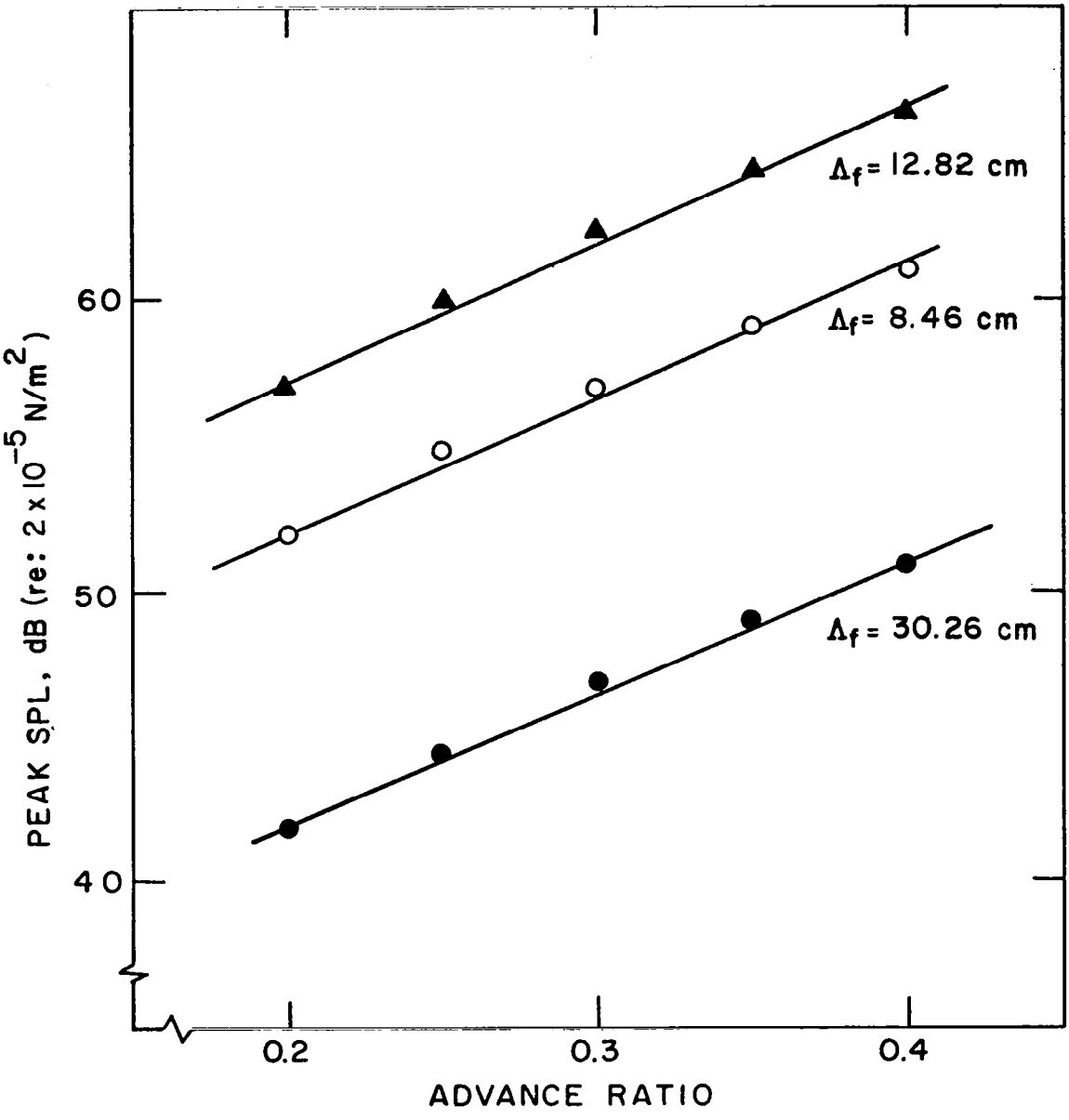

Figure 16.- Effect of advance ratio on the peak intensity of low frequency broadband noise.

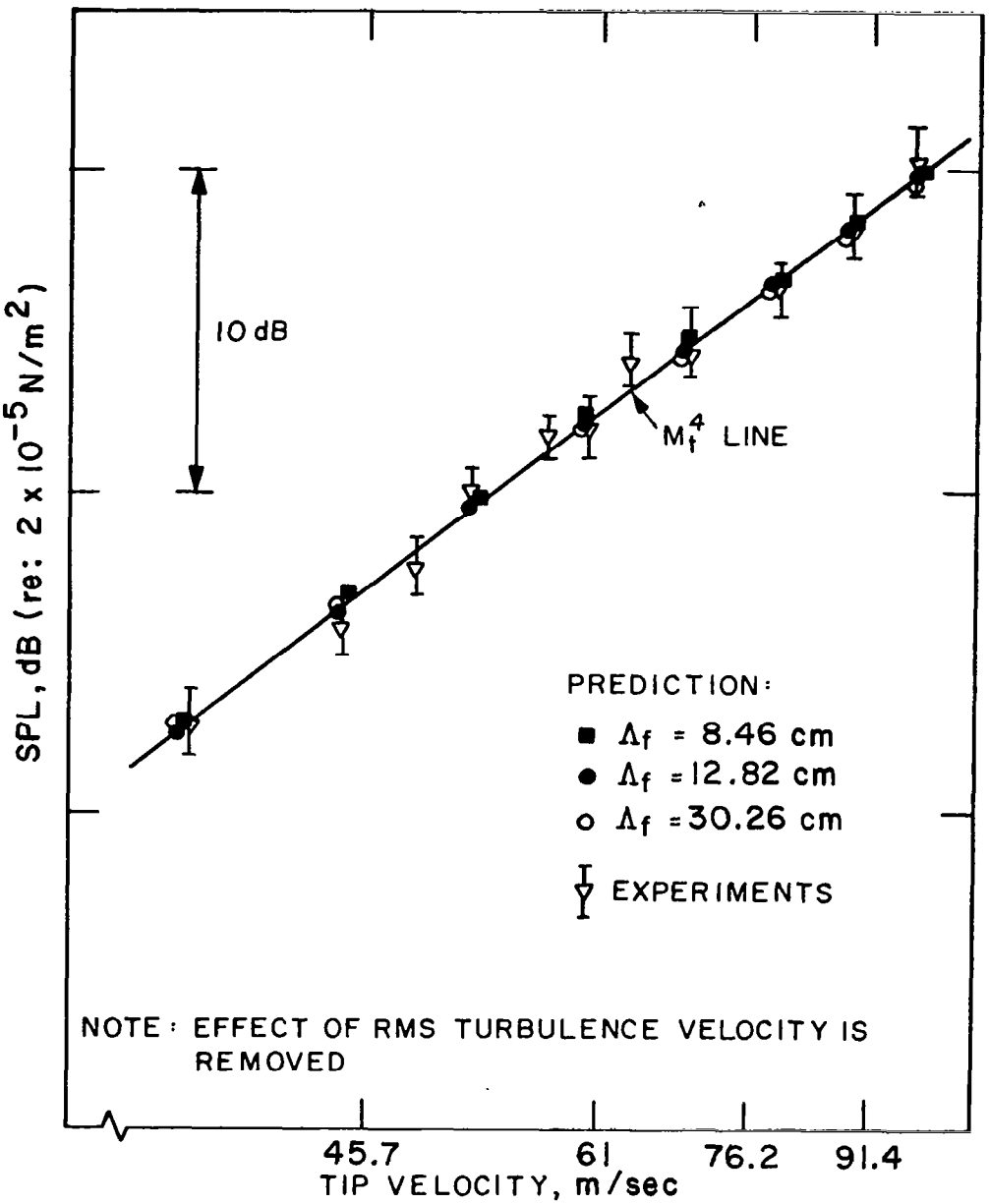

Figure 17.- Effect of tip velocity on predicted and measured peak low frequency broadband noise intensity.

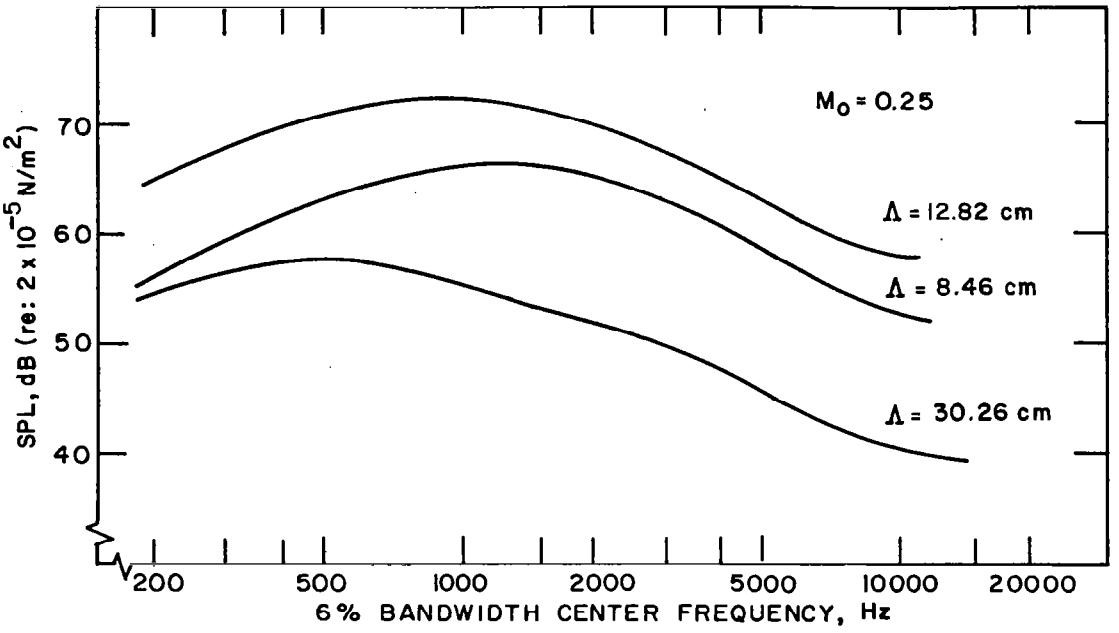

Figure 18.- Effect of integral scale on predicted low frequency broadband noise spectra for M_o = 0.25.

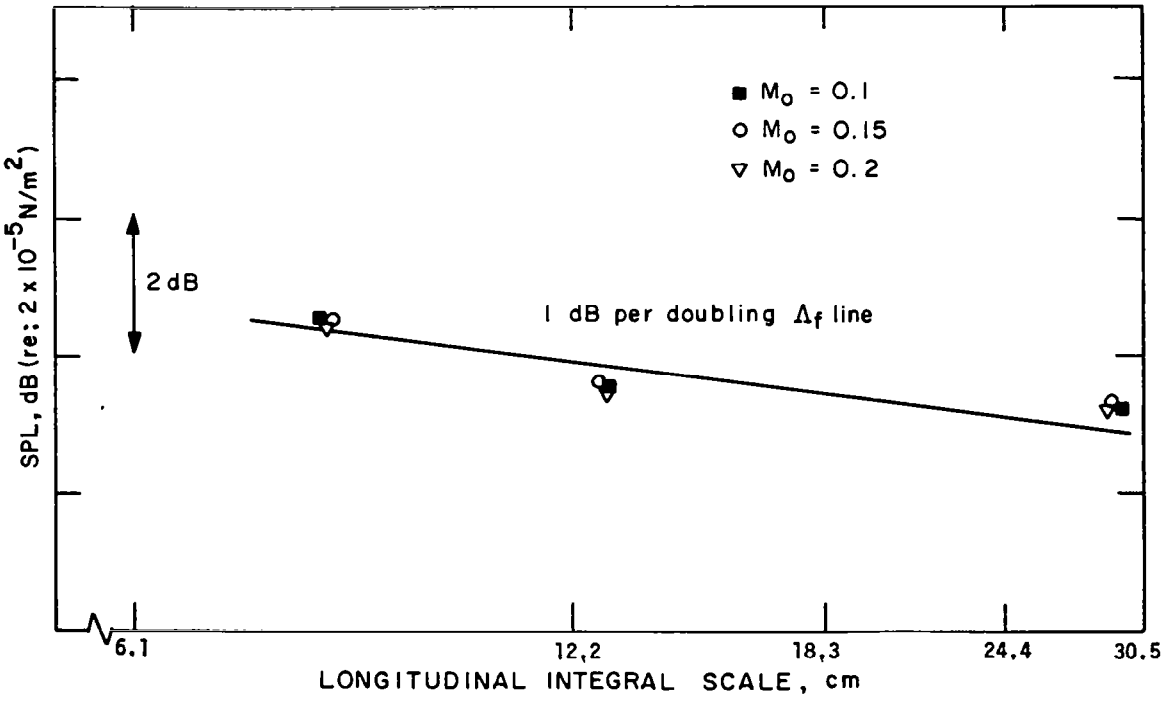

Figure 19.- Effect of turbulence scale on the peak intensity of low frequency broadband noise.

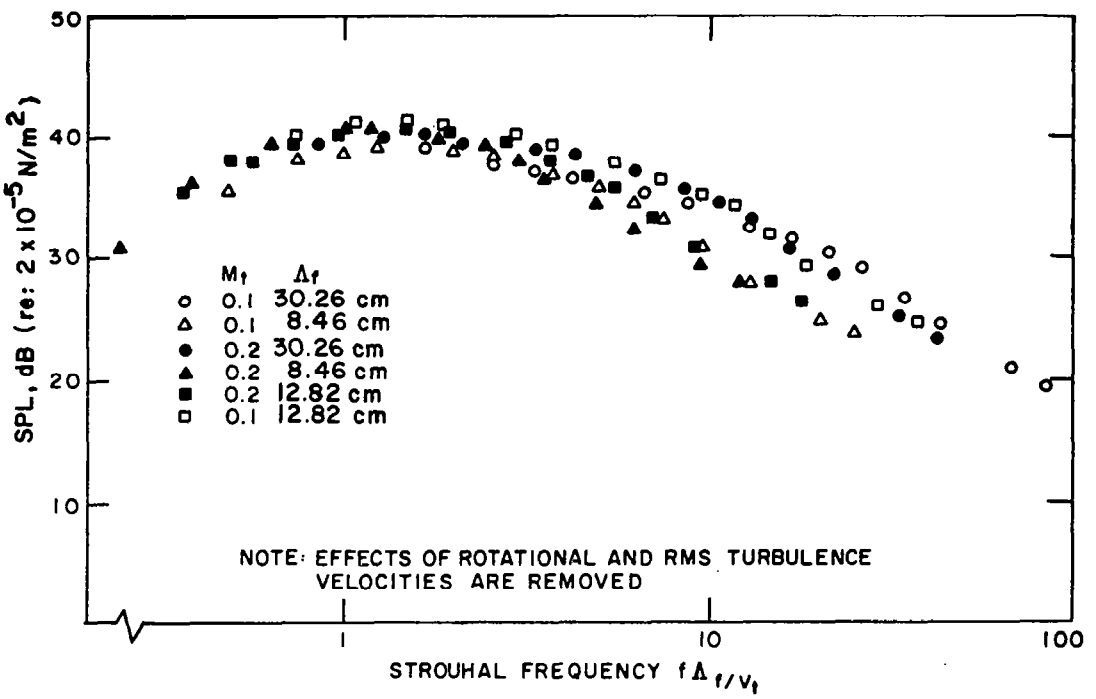

Figure 20.- Spectrum of low frequency broadband noise as a function of nondimensional frequency.

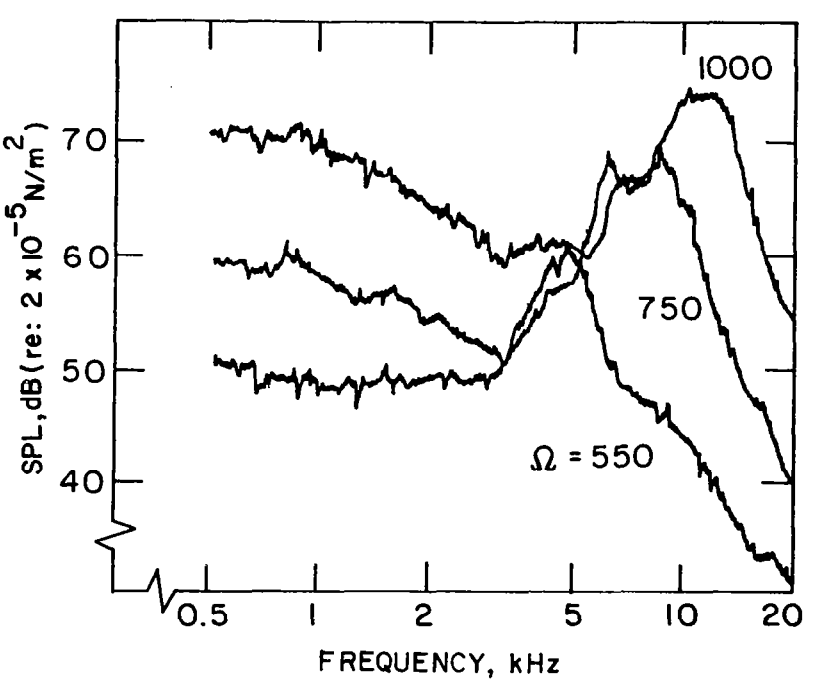

Figure 21.- Typical spectra of high frequency broadband noise at various rotational speeds.

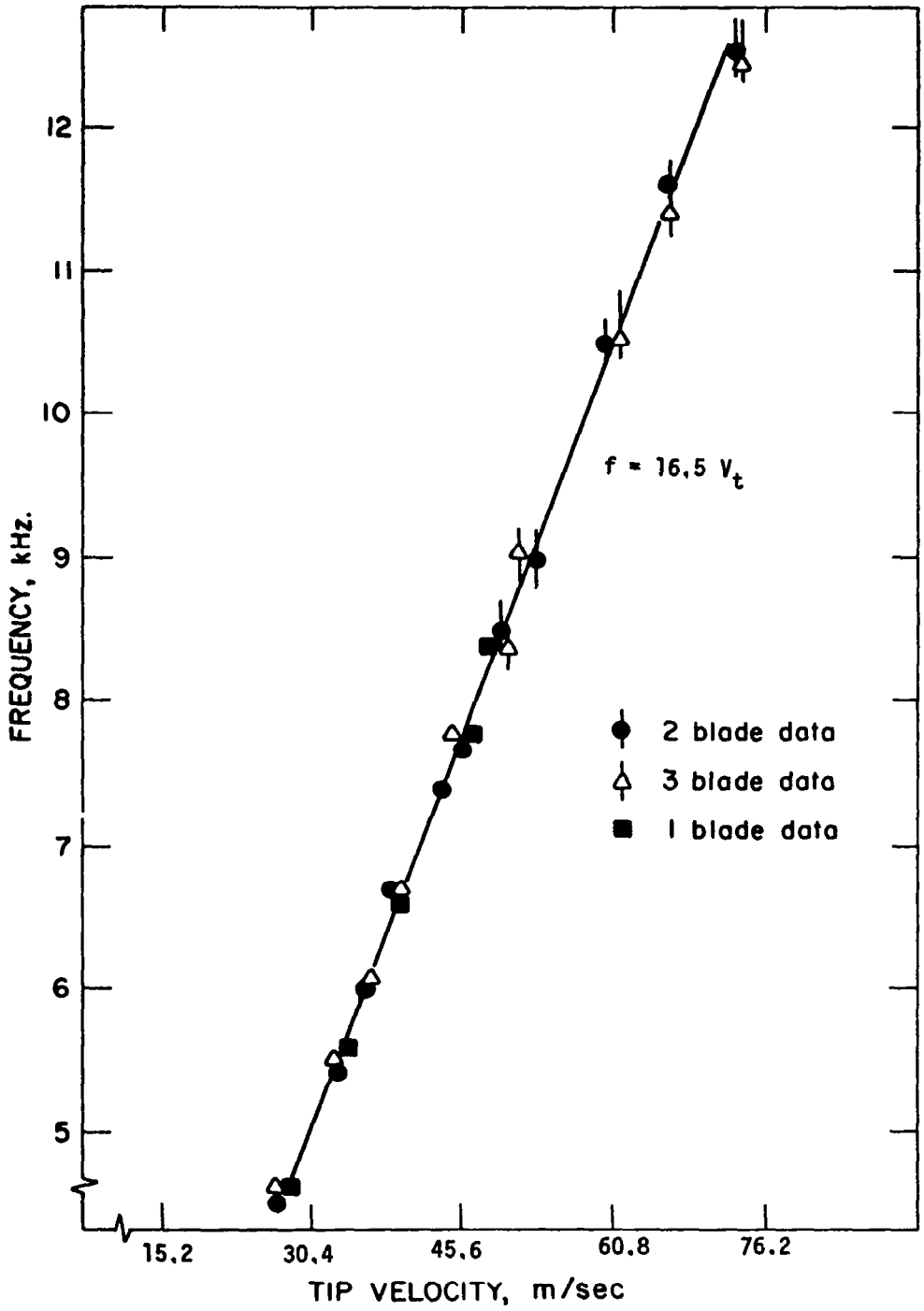

Figure 22.- Peak frequency location as a function of blade tip speed.

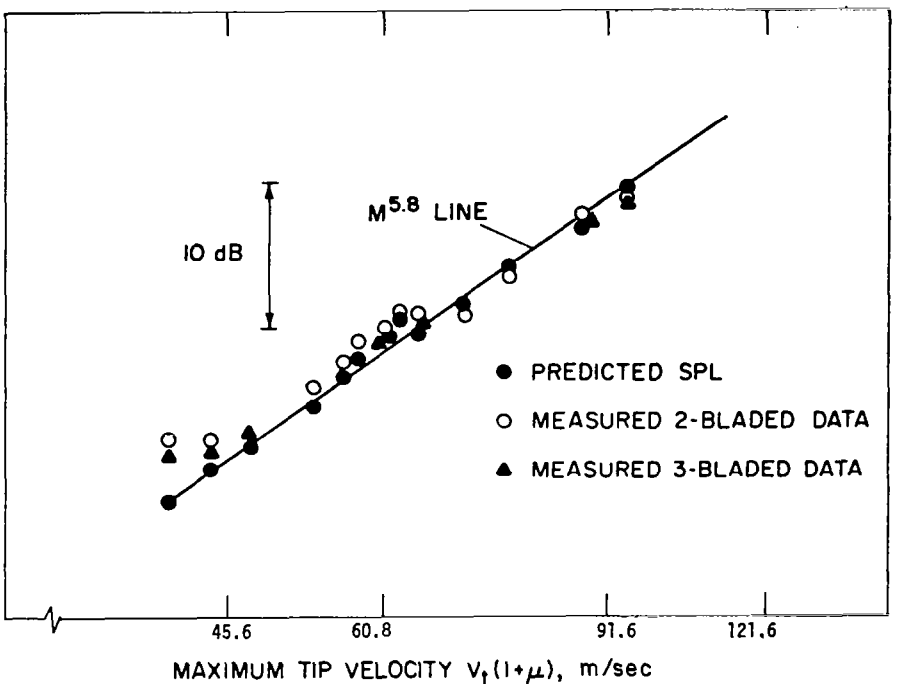

Figure 23.- Velocity scaling of high frequency broadband noise.

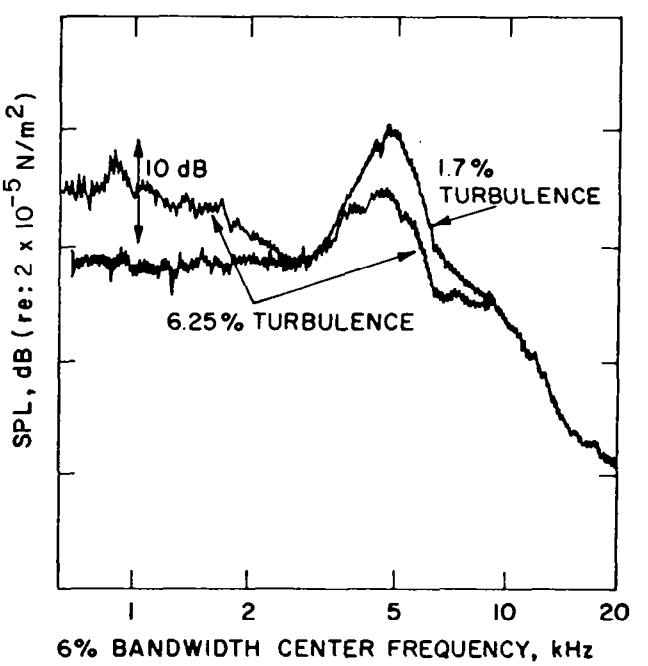

Figure 24.- Effect of free stream turbulence on spectra of high frequency broadband noise.

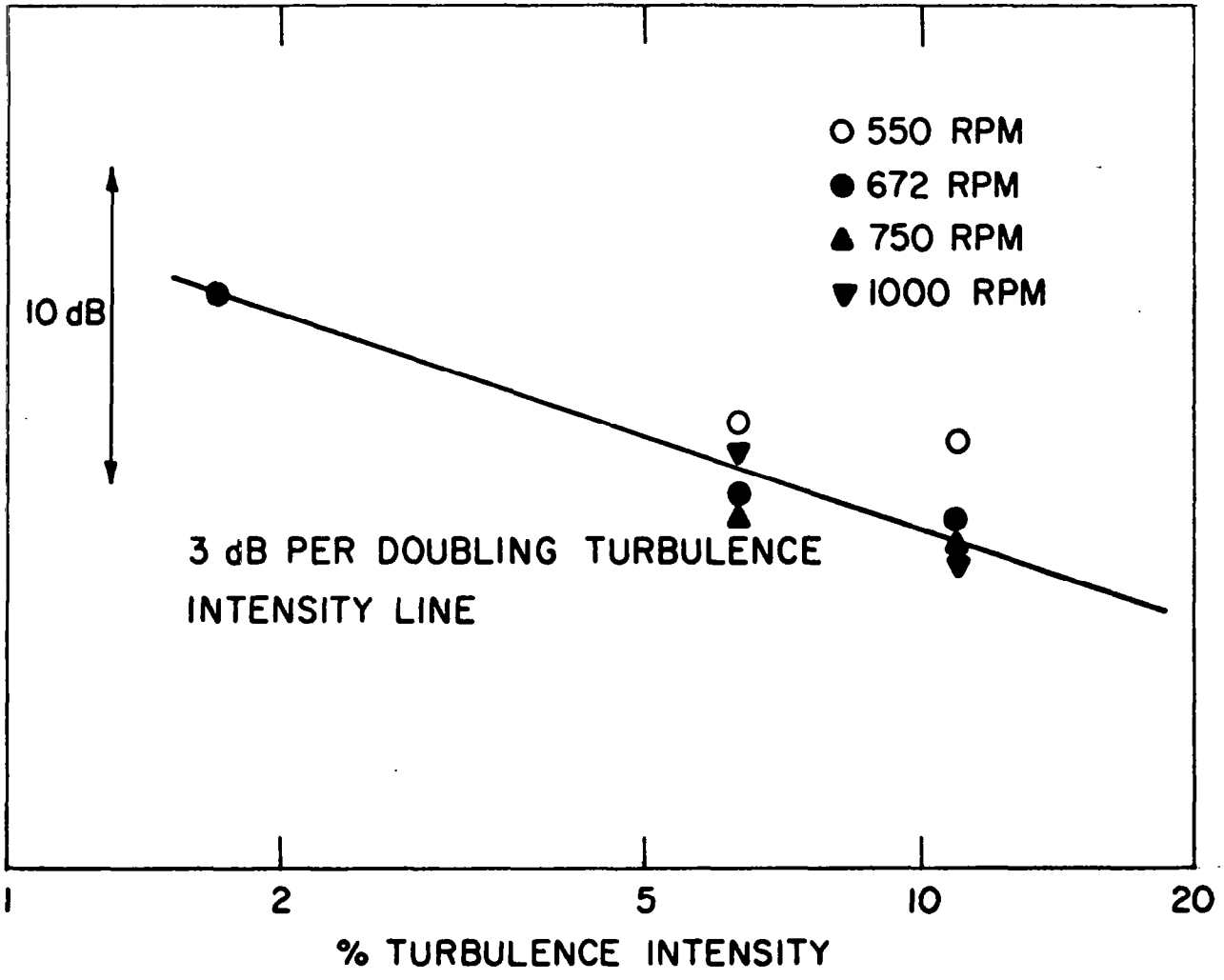

Figure 25.- Effect of free stream turbulence on peak intensity of high frequency broadband noise.